Title: Regulatory variants drive Hsp90's effect on adaptation

Authors: Christopher M. Jakobson[1,4], José Aguilar-Rodríguez[1,2,4], and Daniel F. Jarosz[1,3]*

Affiliations: [1]Department of Chemical and Systems Biology, Stanford University School of Medicine, Stanford, CA, USA [2]Department of Biology, Stanford University, Stanford, CA, USA [3]Department of Developmental Biology, Stanford University School of Medicine, Stanford, CA, USA [4]These authors contributed equally. *To whom correspondence should be addressed: jarosz@stanford.edu

Summary: The essential, stress-responsive protein chaperone Hsp90 impacts adaptation from microbes to humans. Yet the molecular mechanisms involved remain unclear and are often presumed to be driven by variation in opening reading frames. Here, we identify over 1,000 natural genotype-to-phenotype associations governed by Hsp90 at single-nucleotide resolution in *Saccharomyces cerevisiae*. Strikingly, *cis*-regulatory variants contributed to the chaperone's effect on heredity more strongly than coding variation. Most of these mutations nonetheless impacted clients of Hsp90 or targets of its direct binding partners. The chaperone's influence was especially potent on evolutionarily young genes, highlighting its influence on variation central to novelty. Synthetic reconstructions and genome editing revealed that Hsp90 may regulate the relationship between activity and phenotype for many dosage-sensitive genes. The unexpected role of the chaperone in buffering the effects of regulatory variants and releasing their consequences under stress suggests a mechanism for its widespread effects on evolution and development.

Keywords

- Hsp90; systems genetics; protein chaperones; natural variation; genotype-phenotype maps; evolution; adaptation; development; epistasis

INTRODUCTION

The phenotypes expressed from the genome are constantly remodeled throughout development and under stress[1], with profound impacts on disease and evolution[2]. The stress-regulated Heat Shock Protein 90 kDa (Hsp90) chaperone has attracted keen interest as a molecular mediator of these effects[3,4]. Hsp90 is a highly expressed[5] 'hub of hubs' that interacts genetically and physically[6] with hundreds of client[7] kinases, ubiquitin ligases, and other signaling factors[8] that are likewise highly connected nodes of regulatory networks. Thus, Hsp90 couples the turnover, steady-state levels, and localization of much of the regulatory proteome[9,10] to environmental stress[11].

As a result, this chaperone has profound impacts on the phenotypic manifestation of genetic variation[11–18]. Hsp90 activity is tightly linked to oncogenesis[19,20] and the Hsp90 chaperone network plays a central role in neurodegeneration[21]. Such effects are not limited to disease: modest impairment of Hsp90 function during development in *Drosophila melanogaster* results in pronounced changes to wings, eyes, and legs[16], phenotypes classically associated with regulatory variation. The lineage specificity of these effects[16,22], as well as those observed in other organisms[17] from yeast to plants, indicates that Hsp90, in addition to its effects on disease variants, controls the fitness consequences of a substantial fraction of natural polymorphisms. Moreover, this influence is most pronounced under stress when protein quality control is compromised[23]—and when the value of phenotypic novelty is greatest.

However, owing to the limitation of existing genetic mapping technologies, the precise underlying mutations whose effects are modified by Hsp90 have remained obscure in all but a handful of instances[14]. Because Hsp90 is a chaperone of protein folding, prior studies examining the interactions between Hsp90 and, variously, gene deletions[24,25], naturally segregating

49 haplotypes[26], Fanconi anemia mutations[14], variants underlying Mendelian disorders[27], and
50 genotypes harboring small numbers of nearly random mutations[13] made the pragmatic assumption
51 that chaperone-dependent phenotypes arose primarily from coding variation. Yet the
52 morphological and other developmental traits impacted when the chaperone's activity is
53 compromised are most frequently caused by *cis*-regulatory variation[28].

54 Here, we take advantage of the deep conservation of the molecular activity and clientele of
55 Hsp90[29] and the power of quantitative genetics in the budding yeast *Saccharomyces cerevisiae* to
56 identify, at unprecedented scale, hundreds of natural polymorphisms whose effects depend
57 strongly on Hsp90 function. The advent of genetic mapping approaches in *S. cerevisiae* that dissect
58 complex traits to their underlying causal variants[30,31], in conjunction with collections of wild
59 isolates[32,33], genome engineering tools[34,35], and systematic knowledge of genetic and physical
60 interactions[36,37] and the targets of key Hsp90 clients[38–40], make this an ideal venue to understand
61 the mechanisms by which the chaperone reshapes phenotypes. In contrast to prevailing
62 assumptions, we found that even though Hsp90 is a protein chaperone, its effects were most
63 pronounced for non-coding variation. This surprising role in the phenotypic expression of *cis*-
64 regulatory variation provides a mechanistic explanation for Hsp90's potent impact on the evolution
65 of developmental phenotypes. Indeed, buffering the consequences of excursions in activity and
66 releasing their fitness effects under stress may facilitate the accumulation of environmentally
67 specific adaptive variation across Eukarya.

68 **RESULTS**

69 ***Comprehensive mapping of Hsp90-dependent phenotypes***

70 To enable genetic mapping with high resolution and sensitivity, we employed ~15,000 fully
71 genotyped progeny[30] from an F_6 intercross between two wild *Saccharomyces cerevisiae*
72 parents[31,41]: RM11, isolated from a California vineyard[42], and YJM975, isolated from an
73 immunocompromised patient[43]. Although most genes are polymorphic in this mapping panel,
74 those encoding Hsp90—*HSC82* and *HSP82*—are not (mutations in these genes could confound
75 mapping). To assess Hsp90's impact on phenotypes driven by the diverse natural variants present
76 in this cross [**Fig. 1A**], we used a potent and specific natural product inhibitor, radicicol[44], at a
77 dose that reduced but did not eliminate chaperone activity[18] [**Fig. S1A**], did not perturb growth in
78 the absence of stress [**Fig. S1B**], and did not induce a bounce-back heat shock response[26] [**Fig.**
79 **S1CD**].

80 We first examined the growth of the 15,000 diploid progeny in response to diverse
81 environmental perturbations (including alternate carbon sources, toxic metal ions, and DNA-
82 damaging agents, as well as antifungal drugs used clinically and in agriculture) [**Supplemental**
83 **Table S1**]. Parallel experiments in the presence of radicicol revealed that Hsp90 inhibition
84 dramatically altered the growth of many progeny [**Fig. 1B**], but did so in a manner that was highly
85 specific to genotype and environment [**Fig. S1E**]. Coarse genetic mapping readily identified loci
86 with Hsp90-dependent phenotypic effects logically connected to the traits we examined [**Fig. 1C**],
87 including the rapamycin-resistance phenotype of a locus centered about the *AVO3*
88 (*TSC11*/RICTOR[45]) gene [**Fig. 1D**] – the Avo3 protein is a key component of the TORC2 complex,
89 a direct target of rapamycin.

90 To investigate whether our findings from this defined mapping panel generalized across
91 distinct genetic backgrounds, we assessed how Hsp90 inhibition influenced growth in rapamycin
92 across > 1,000 wild yeast isolates[33] from diverse ecological niches and geographic origins.
93 Resistance associated with the clinical allele of Avo3, and its Hsp90-dependence, was apparent
94 across the >100 wild isolates that harbored this allele amidst additional variation at more than one
95 million other loci [**Fig. 1E**]. Although genetic background can exert a strong influence on
96 phenotype, these observations suggest that inferences about Hsp90's relationship to the effects of
97 specific genetic variants from our experiments may hold across a very wide range of wild isolates.
98

99 ***Hsp90 is a potent buffer of regulatory variation***

100 Integrating over 1,000,000 growth measurements and employing a multivariate mapping
101 procedure[30], we identified more than 5,000 Hsp90-dependent loci throughout the genome,
102 exceeding the number previously identified by orders of magnitude [**Supplemental Table S2**],
103 and emphasizing Hsp90's widespread influence on the heredity of diverse biological traits. Our
104 mapping approach provided a comprehensive picture of Hsp90-dependent heredity, revealing that
105 up to 76.2% of Hsp90's effect on fitness was due to changes in the phenotypic effects of genetic
106 variation [**Fig. S1FG**]. Consistent with the minimal effect of radicicol on growth in the absence of
107 stress, no more than 20% of the Hsp90-dependent QTLs in any environment overlapped with those
108 identified in the no-stress condition, and even less so for the strongest-effect loci. The expression
109 of Hsp90 itself also made a minor contribution: the lone regulatory variant near either the *HSC82*
110 or *HSP82* genes explained only 0.08% of Hsp90-dependent growth. Moreover, only two of the
111 Hsp90-dependent loci we identified overlapped with Hsf1 binding sites [**Supplemental Table S2**],
112 further confirming that the heat shock response was not engaged.

113 We classified Hsp90-dependent loci into two broad categories. In the first, known as
114 buffering interactions, the phenotypic effect of an allele is masked by Hsp90 and thus *increased*
115 upon radicicol treatment, a release of cryptic variation sometimes termed decanalization[46,47]. In
116 the second, known as potentiation interactions, the phenotypic effect of a variant is dependent on
117 Hsp90 and thus *reduced* upon radicicol treatment (as with the transforming kinase v-Src[18]) [**Fig.**
118 **S1H**]. Across the 1,154 interactions (that is, Hsp90-dependent effects on phenotype) that we
119 identified, both behaviors were common. Buffering interactions were somewhat stronger than
120 potentiations (median 15%; $p < 10^{-4}$) [**Fig. S1I**], and we noted that Hsp90 inverted the fitness
121 effects of 309 variants. Although they were a minority of the interactions we observed, the average
122 effect size of such inversions was large [**Fig. S1J**] and may explain the 'line-crossing' Hsp90
123 dependence that has been reported for randomly accumulated mutations[13]. Overall, the magnitude
124 of Hsp90's impact on individual variants (median variance explained ~ 0.21%) was comparable
125 to the phenotypic contributions of the variants themselves (~ 0.26%) [**Fig. S1K**] and, when Hsp90
126 was inhibited, buffered variants exhibited the largest effects [**Fig S1L**]. The majority of these
127 effects far exceed the threshold for effective neutrality in this organism ($s \sim 10^{-8}$ - 10^{-6})[48],
128 establishing that Hsp90 is poised to impact the evolutionary fate of a broad swath of natural genetic
129 variation. Consistent with reduced selection on variants that are typically buffered, allowing them
130 to reach fixation more often, alleles buffered by Hsp90 rose to higher frequencies in *S. cerevisiae*
131 than variants that were causal with Hsp90 active ($p < 0.01$); the same was not true of potentiated
132 alleles ($p = 0.27$) [**Fig. S1M**].

133 To pinpoint the polymorphisms responsible for Hsp90-dependent traits, we performed
134 high-resolution genetic mapping[31,41,49] of the change in growth upon chaperone inhibition across
135 each environmental perturbation. These nucleotide-resolution data revealed that nearly half (542

136 of 1,154) of the fine-mapped variants were outside of annotated open reading frames. Moreover,
137 regulatory variants accounted for more Hsp90-dependent heredity than protein-altering variants
138 [**Fig. 1FG; Fig. S1N**], even though only 30% of the yeast genome is noncoding and only 44% of
139 the SNPs in our mapping panel lie outside open reading frames.

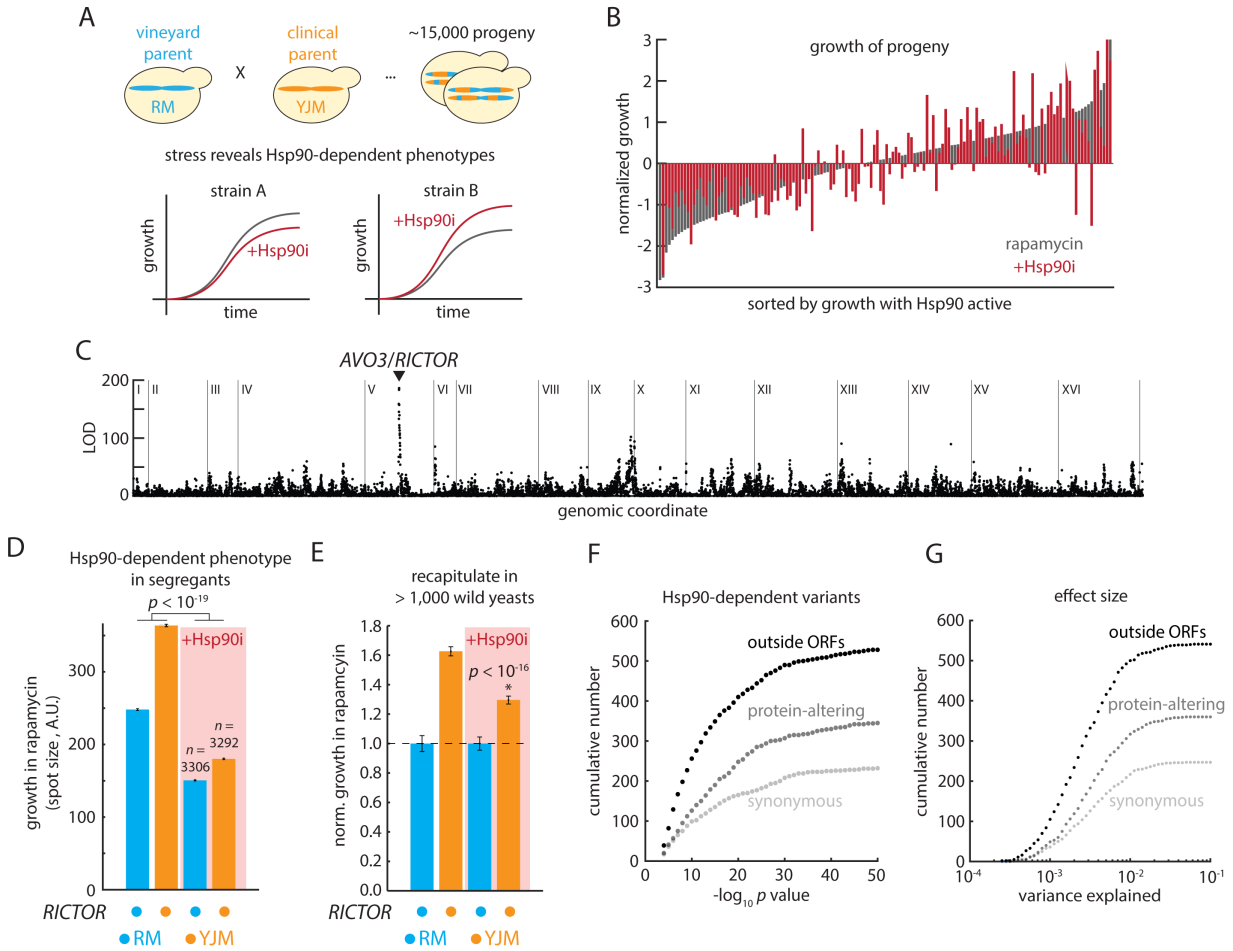

Figure 1. Mapping the basis of Hsp90-dependent phenotypes. (A) Schematic of genetic mapping population and hypothetical Hsp90-dependent phenotypes of different strains. (B) Rank-ordered normalized growth of 146 randomly selected progeny in rapamycin, with (red) and without (gray) radicicol. Data are normalized to mean = 0 and standard deviation = 1 amongst the F_6 progeny in that treatment condition. (C) Manhattan plot of univariate genetic mapping of Hsp90-dependent rapamycin resistance. Loci are in genomic order, with chromosomes as indicated. LOD, log of the odds distribution. 5% FDR threshold < 5 by permutation. (D) Growth in rapamycin with (red shading) and without (no shading) radicicol of progeny bearing the sensitive (blue) and resistant (orange) alleles of Avo3/RICTOR. Data shown are mean and s.e.m. for the indicated number of progeny with each homozygous genotype; *F* test *p*-value from multivariate regression. (E) Replication of the Hsp90-dependent phenotype in wild isolates sorted by their Avo3 genotype as indicated: $Avo3^{Thr1342}$ in blue (n = 152) and $Avo3^{Lys1342}$ in orange (n = 806). Growth was measured with Hsp90 active (no shading) and inhibited (red shading) Data shown are mean and s.e.m. normalized to the growth of the RM11 $Avo3^{Thr1342}$ allele; *p* value by *t* test relative to growth without radicicol. (F) Cumulative frequency plots of multivariate regression *p* values for protein-altering, synonymous, and regulatory Hsp90-modified variants. (G) Cumulative frequency plots of multivariate regression variance explained for protein-altering, synonymous, and regulatory Hsp90-modified variants. See also [**Fig. S1**].

159 ***Reconstruction by gene editing to confirm the nucleotide-resolution map***

160 To confirm the findings from our mapping analyses, we first used genome editing to reconstruct a
161 SNP in Avo3[50] linked to Hsp90-dependent rapamycin resistance [**Fig. 2A**]. Statistical fine
162 mapping suggested that a missense variant at position 1342 of the Avo3 protein was likely
163 responsible, as indicated by a pronounced peak in the QTN score (although, notably, not in the
164 traditional LOD metric). Examining the predicted structure[51] of this Hsp90 client[36], we noted a salt
165 bridge formed by the polymorphic Lys1342 residue that appeared to stabilize the region of
166 Avo3/RICTOR that renders TORC2 insensitive to rapamycin[52] [**Fig. 2B**]. Consistent with this
167 hypothesis, introduction of the alternate Thr1342 allele found in the RM11 vineyard parent by
168 gene editing conferred pronounced rapamycin sensitivity that was attenuated by radicicol
169 treatment [**Fig. 2C**]. By contrast, introduction of the Lys1342 allele found in the clinical parent
170 conferred potentiated resistance [**Fig. 2C**]. We obtained similar results with radicicol and the
171 structurally and mechanistically distinct Hsp90 inhibitor geldanamycin[53], and neither variant
172 strongly influenced growth in the absence of rapamycin [**Fig. S2A**], confirming that the
173 phenotypes of these polymorphisms were transformed by Hsp90 activity.

174 Next, to better understand the surprising enrichment for Hsp90-dependent regulatory
175 variants, we investigated a T>C variant 206 base pairs upstream of the *ERG11* transcription start
176 site[54] [**Fig. 2D**] linked to Hsp90-buffered resistance to the antifungal drugs tebuconazole and
177 fluconazole, which inhibit Erg11 and are widely used in agriculture[55] and the clinic[56] [**Fig. S2B**].
178 Genomic reconstruction of the regulatory SNP recapitulated its chaperone-dependent effect on
179 sensitivity to these mainline antifungal drugs [**Fig. 2E; Fig. S2C**]. The mutation had a negligible
180 effect on growth in the absence of drug, regardless of Hsp90 activity [**Fig. S2D**]. The results of

181 these genome editing studies establish that drug resistance was due to a buffering interaction

182 between this regulatory variant and Hsp90, a chaperone of protein folding.

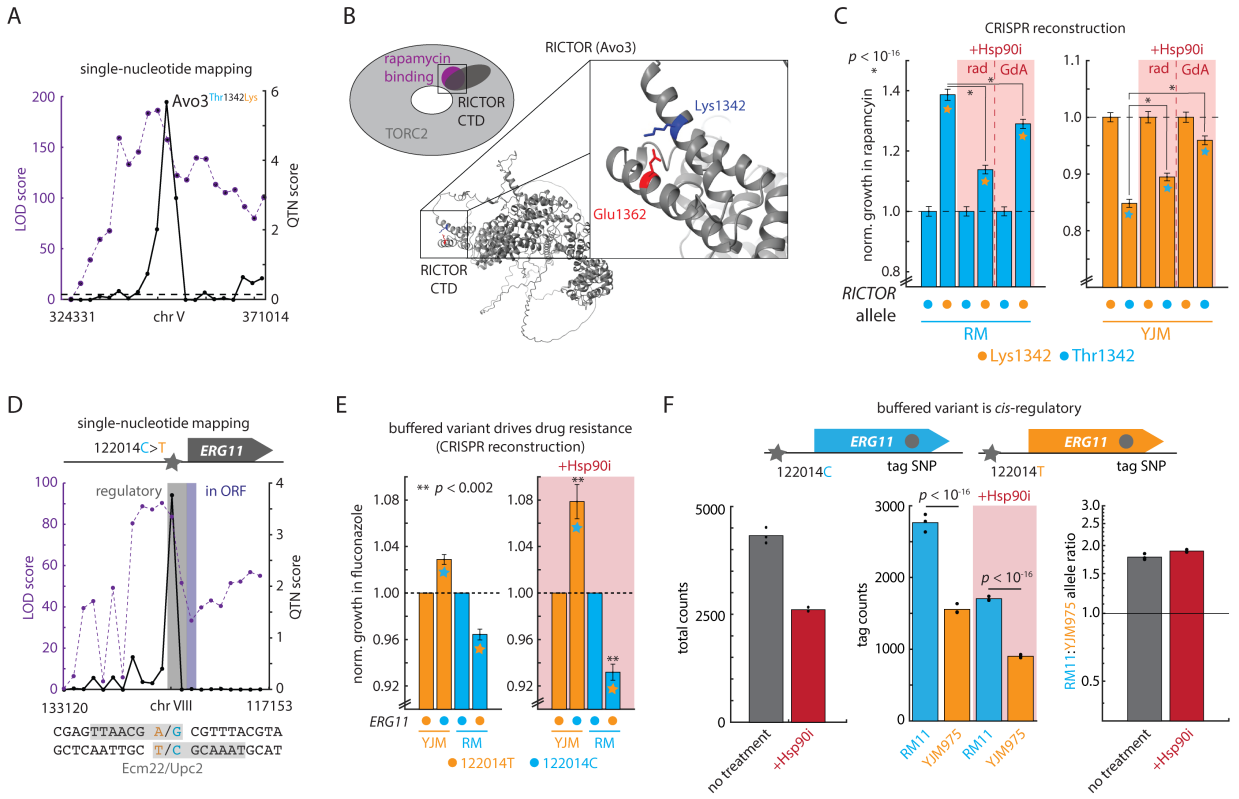

Figure 2. Identifying individual genetic variants underlying Hsp90-dependent phenotypes. (A) Univariate genetic mapping of Hsp90-dependent rapamycin resistance (LOD score; left ordinate) overlaid with multivariate fine-mapping (ANOVA QTN score; right ordinate) of the same phenotype, highlighting the causal variant Avo3^{Thr1342Lys}. (B) Schematic of the TORC2 complex, rapamycin binding pocket, and RICTOR C-terminal domain; Alphafold2 predicted structure of Avo3, highlighting the causal residue Avo3^{Lys1342} and its proximity to Avo3^{Glu1362}. (C) Growth in rapamycin of genome-edited strains with Hsp90 active (no shading) and inhibited (red shading). The right panel shows wild type RM11 Avo3^{Thr1342} strains and edited RM11 Avo3^{Lys1342} strains (orange stars); the left panel shows wild type YJM975 Avo3^{Lys1342} and edited YJM975 Avo3^{Thr1342} strains (blue stars). Hsp90 was inhibited with both radicicol (rad) and geldanamycin A (GdA). Data shown are mean and s.e.m. normalized to the wild type; *p* values by *t* test; $n = 96$ per genotype. (D) Univariate genetic mapping of Hsp90-dependent fluconazole resistance (LOD score; left ordinate) overlaid with multivariate fine-mapping (ANOVA QTN score; right ordinate) of the same phenotype, highlighting the causal variant *ERG11*$^{122014C>T}$. Indicated below are overlapping near-cognate binding sites for Ecm22/Upc2 centered about the polymorphism. (E) Growth in fluconazole of genome-edited strains in fluconazole with (red shading) and without (no shading) Hsp90 inhibition with radicicol (+Hsp90i). Each panel shows wild type YJM975 *ERG11*^{122014T}, edited YJM975 *ERG11*^{122014C} (blue stars), wild type RM11 *ERG11*^{122014C}, and edited RM11 *ERG11*^{122014T} (orange stars) strains. Mean and s.e.m. are shown, normalized to the wild type; *p* values by *t* test against the same mutant strain without radicicol treatment; $n = 384$ per genotype. (F) Top: Schematic of *ERG11* alleles in the hybrid diploid; indicated are the Hsp90-dependent 122014C>T regulatory variant and the Erg11^{Lys433Asn} tag SNP. Below left: Total counts at the Erg11^{Lys433Asn} tag SNP with Hsp90 inhibited with radicicol (red) or Hsp90 active (grey).

Below middle: estimated counts at Erg11^{Lys433Asn} tag SNP for the RM11 allele (blue) and the YJM975 allele (orange) with Hsp90 inhibited with radicicol (red shading) or Hsp90 active. Bars show mean and dots show replicates. Below right: Mean allelic ratio (RM11 counts/YM975 counts) at the Erg11^{Lys433Asn} tag SNP with Hsp90 inhibited with radicicol (red) or Hsp90 active (grey). Bars show mean and dots show replicates; p values by binomial test; $N = 3$. See also [**Fig. S2**].

213 ***Hsp90 controls the phenotypic effects of* cis*-regulatory variation***

214 We initially hypothesized that Hsp90 might alter how these SNPs impact mRNA levels, and
215 therefore investigated allele-specific mRNA expression in the heterozygous diploid parent of our
216 genetic mapping panel. This approach capitalizes on polymorphisms in transcribed regions that
217 'tag' transcripts as originating from either the RM11 or YJM975 parental chromosomes [**Fig.**
218 **S3A**]. A predominance of one haplotype over the other indicates the presence of a *cis*-acting
219 regulatory variant at that gene[57]. Roughly a quarter of all non-coding variants with phenotypes that
220 were impacted by Hsp90 (107 of 451) exhibited significant allele-specific expression (ASE) when
221 the chaperone was inhibited (amongst ORFs with tag SNPs; Bonferroni-corrected $q < 0.05$; see
222 **Methods**, **Fig. S3B**, and **Supplemental Table S3**). The buffered variant at *ERG11*, for instance,
223 showed pronounced RM11-biased expression (RM:YJM allelic ratio = 1.78 ± 0.06) [**Fig. 2F**]. This
224 *cis*-regulatory effect was consistent with the variant's proximity to two near-cognate Ecm22/Upc2
225 binding motifs near the start of *ERG11* transcription [**Fig. 2D**][58] and our observation that the RM11
226 allele conferred azole resistance [**Fig. 2A**]. Hsp90 inhibition markedly decreased the overall level
227 of *ERG11* expression, possibly because the Upc2 transcription factor associates with Hsp90[59]. Yet
228 the biased allelic expression was preserved (1.89 ± 0.03) [**Fig. 2F**].

229 Indeed, Hsp90 inhibition rarely had a strong effect on ASE—only 18% of Hsp90-
230 dependent SNPs changed in allelic ratio by more than 50%—despite often affecting expression in
231 *trans* [**Fig. 3A**; **Fig. S3C**]. As with the *ERG11* mutation, the largest and most frequent effects we
232 identified across the genome arose from variants upstream of the TSS, consistent with altered
233 transcription factor recruitment or transcription initiation [**Fig. 3B**]. 123 Hsp90-dependent
234 variants, however, were in the predicted 3' UTR of mRNAs and 55 in the 5' UTR [**Fig. 3C**],
235 pointing to a significant role for post-transcriptional regulation. For example, a polymorphism that

236 caused Hsp90-dependent resistance to both lithium and nickel stress localized to the highly
237 structured 3' UTR[60] of *HAC1*, which regulates pre-mRNA splicing and levels *via* Ire1[61]. Likewise,
238 numerous Hsp90-dependent phenotypes arose from the 3' UTR of the cysteine desulfurase gene
239 *NFS1*, which exhibits nutrient-dependent interactions with RNA-binding proteins[62]. Introducing a
240 G>A polymorphism 61 base pairs downstream of *NFS1* by gene editing was sufficient to confer
241 pronounced buffered sensitivity to fluconazole and concomitant buffered resistance to the DNA-
242 damaging agent doxorubicin, confirming the role of this 3' UTR in chaperone-dependent heredity
243 [**Fig. 3D**].

244 Interestingly, we previously implicated coding variation in Nfs1 in Hsp90-buffered
245 rapamycin resistance arising in a different segregant panel[26]. These observations, in conjunction
246 with the modest effect on ASE, led us to hypothesize that the nature of Hsp90's impact on genetic
247 variation may be a gene-level property in which the chaperone controls fitness effects by enhancing
248 the amount of folded, active protein that is produced, thereby limiting the phenotypic impact of
249 *cis*-regulatory effects. Indeed, despite having little effect on mRNA ASE itself, Hsp90 more
250 strongly impacted the consequences of potent regulatory variants (polymorphisms associated with
251 significant allelic imbalances; $q < 0.05$) [**Fig. S3D**].

252 We also noted that more than 200 Hsp90-modified variants were synonymous – that is,
253 they represented a change in codon choice but not in protein sequence. Of these, 38 of 247 (~ 15%)
254 exhibited mRNA allele-specific expression. As expected, this was a much lower fraction than for
255 regulatory variants, which we expect to act predominantly on mRNA (~ 29%). Consistent with
256 roles for both mRNA- and protein-level regulation, synonyms with mRNA ASE did not exhibit
257 larger effect sizes than synonymous variants with no ASE [**Fig. S3E**]. Thus, many of the Hsp90-
258 interacting synonymous variants may drive phenotypes via protein levels or co-translational

259 folding. Synonyms without ASE that interacted with Hsp90 indeed exhibited larger changes in
260 normalized translational efficiency (nTE; a statistic that estimates codon optimality based on
261 codon usage and tRNA availability[63]) than Hsp90-dependent synonyms with ASE (which
262 presumably act at the mRNA level) [**Fig. S3E**], further suggesting that protein-level effects may
263 play a role for these variants. On the other hand, synonyms with ASE were closer to protein domain
264 boundaries than those without [**Fig. S3E**], potentially suggesting a role for changes in translation
265 rate and co-translational folding feeding back onto mRNA stability[64]. Thus, synonyms likely
266 constitute an additional form of *cis*-regulatory variant within the open reading frame, analogous to
267 *cis*-regulatory variants outside ORFs that control mRNA expression.

268 Proteins are typically present at levels that do not limit growth[65]; however, their
269 destabilization upon Hsp90 inhibition might elicit dosage sensitivity, which, in turn, would reveal
270 newfound phenotypes derived from the pre-existing molecular consequences of buffered *cis*-
271 regulatory variants. Consistent with this idea, we found that buffering interactions were stronger
272 than potentiations amongst variants associated with mRNA *cis*-regulation (median 63% larger; p
273 < 0.03) [**Fig. 3E**; **Fig. S3F**]. Studies in diverse organisms have illustrated the potential for Hsp90
274 to have profound and lineage-specific consequences for developmental phenotypes[17] typically
275 associated with *cis*-regulatory variation, often involving the release of cryptic phenotypic diversity.
276 Our results suggest that these buffering interactions may naturally and frequently arise from the
277 confluence of *cis*-acting variants with the widespread consequences of Hsp90 on the folding and
278 activity of proteins at the core of eukaryotic regulatory circuitry.

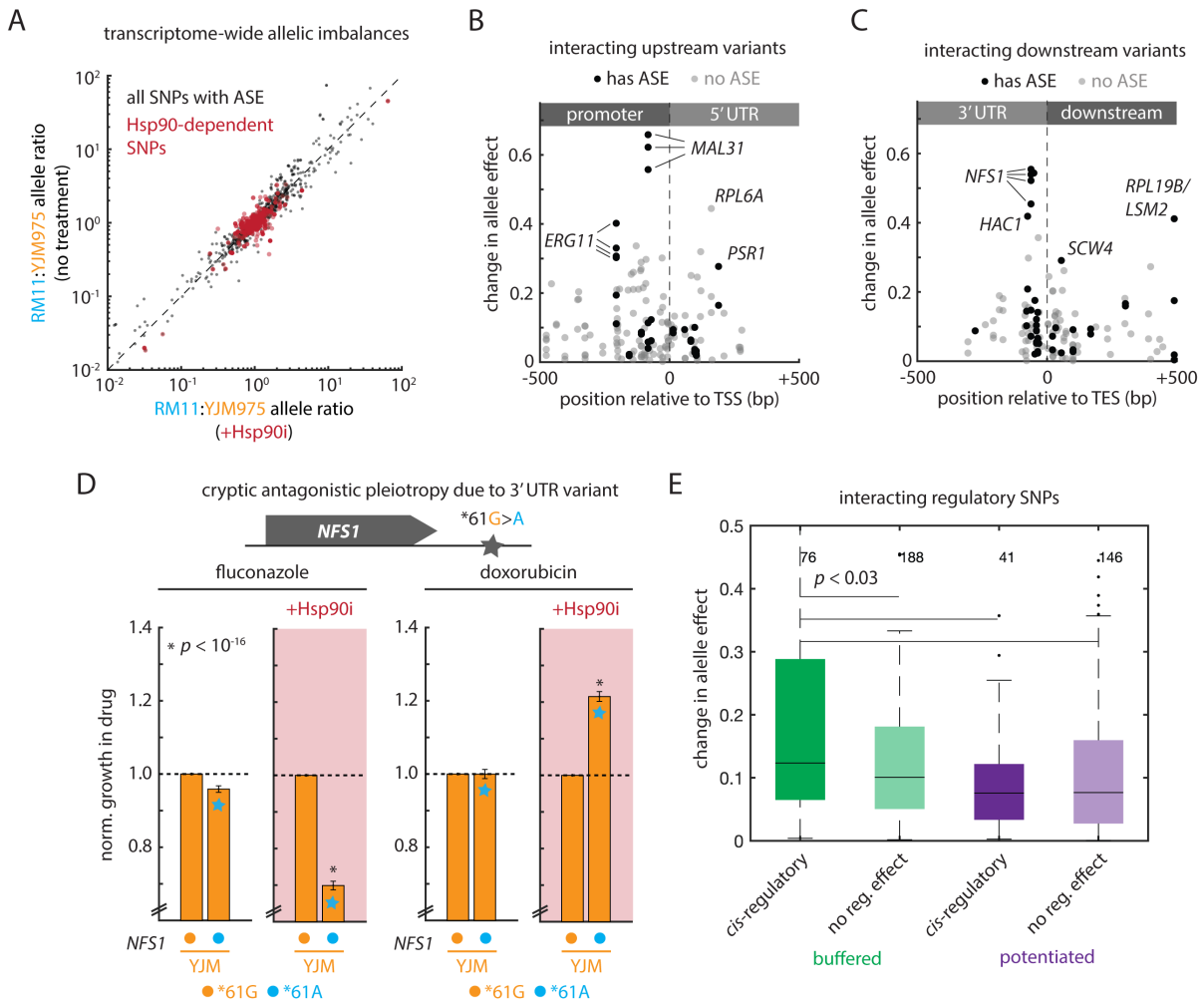

Figure 3. Hsp90 controls the phenotypic outcomes of *cis*-regulatory variation. (A) Allelic ratio (RM counts/YJM975 counts) in the hybrid diploid with Hsp90 inhibited by radicicol (abscissa) or with Hsp90 active (ordinate) for all SNPs with genome-wide significant allele-specific expression (grey) and for SNPs with Hsp90-dependent phenotypic effects (red). Mean allelic ratios are shown across three replicates for each condition. (B) Schematic illustrating the position of upstream Hsp90-modified regulatory variants relative to the TSS of the nearest gene; genome-wide significant allele-specific expression is as indicate (black dots: SNP has ASE [$q < 0.05$]; grey dots: no ASE). Selected large-effect alleles are highlighted. (C) As in (B), but for downstream Hsp90-modified regulatory variants relative to the TES. (D) Growth in fluconazole (left) and doxorubicin (right) of genome-edited strains with Hsp90 active (no shading) and inhibited with radicicol (+Hsp90i; red shading). Each panel shows wild type YJM975 *NFS1*^{*61G}, and edited YJM975 *NFS1*^{*61A} (blue stars) strains. Mean and s.e.m. are shown, normalized to the wild type; p values by t test against the same mutant strain without radicicol treatment; n = 384 per genotype. (E) Absolute change in allele effect for Hsp90-modified regulatory variants that were buffered (green) and potentiated (purple), sorted by whether the transcript exhibited allele-specific expression (left) or had a tag SNP but no allele-specific expression (right). Box plots show the median and upper

296 and lower quartiles; whiskers show 1.5 times the interquartile range; *p* values by *t* test; *n* as
297 indicated. See also [**Fig. S3**].

298 ***Hsp90 modifies variation in its clients and their targets***

299 Our observation that both coding and non-coding variants drove Hsp90-dependent phenotypes led
300 us to ask whether either were linked directly to Hsp90's well-characterized chaperone activity
301 [**Fig. 4A**] or instead were connected by complex nonspecific percolation through regulatory
302 circuitry. We initially considered both genetic and physical interactions, as genetic interactions
303 provide information on functional connections that can be challenging to capture physically if the
304 proteins in question are expressed at low levels, or if the relevant interactions are fleeting.
305 Strikingly, modified alleles of all types were much more likely to occur in or regulate genes that
306 interact with Hsp90 (Bonferroni-corrected $q < 10^{-5}$ for Hsc82, $q < 0.001$ for Hsp82) [**Fig. 4B**][66].
307 We also searched the interactors of Hsp70 chaperones, which collaborate with Hsp90 to catalyze
308 the folding of many client proteins, and those of the Hsp70/Hsp90 Organizing Protein
309 (HOP/Sti1[67–69]). These interactors were enriched for modified alleles ($q < 10^{-5}$ for Sti1 and the
310 Hsp70 proteins Ssa1, Ssb1, and Sse1), and the well-characterized Hsp40 adaptor Ydj1 and the
311 kinase co-chaperone Cdc37 exhibited similar enrichments ($q < 10^{-5}$) [**Fig. 4B**]. We also noted
312 enrichments amongst the interactors of the Hsp70 homologue Lhs1 ($q < 0.003$) and Hsp40
313 homologue Xdj1 ($q < 0.02$), suggesting a role for ER and mitochondrial protein quality control in
314 the effects we observed [**Fig. S4AB**]. Although the Hsp90-dependent phenotypes we identified
315 were mechanistically diverse and often driven by *cis*-regulatory variation, most interacting variants
316 (59.8%) occurred in genes that encode direct clients of the Hsp90/Hsp70/Sti1 chaperone system[36]
317 ($p < 10^{-3}$ by Fisher's exact test). In fact, the genes controlled by interacting *cis*-regulatory variants
318 exhibited particularly strong enrichments for both physical and genetic interactors of Hsp90 and
319 related chaperones [**Fig. 4CD**]. This was consistent with the hypothesis that cells are sensitized to

320 the effects of regulatory mutations on mRNA levels when the client proteins they control are
321 destabilized or otherwise functionally compromised.

322 An unbiased analysis to identify the 'hub' genes with the most direct biological
323 connections[66] to the interacting SNPs also highlighted numerous members of the Hsp90/Hsp70
324 chaperone machinery (*e.g.* Hsc82, Hsp82, Ydj1, Ssa1, Ssb1, Cdc37, Sti1) amongst the genes most
325 connected to the Hsp90-dependent fitness effects we mapped [**Fig. 4EF**]. Moreover, 73 of the top
326 100 hubs were themselves interactors of Hsc82 or Hsp82 ($p < 10^{-22}$, Fisher's exact test), illustrating
327 the ubiquity of connections from the 'hub of hubs' Hsp90 to genes throughout the cellular network.
328 Notably, the hub candidates included not only ubiquitin ligase components such as Slx5 and the
329 kinase activator Mob2, but also numerous RNA-binding proteins including Dhh1, Ccr4, and Nab2
330 [**Fig. 4F**]. These interactions may point toward multiple mechanisms linking Hsp90 activity to the
331 outcomes of 3' and 5' UTR variation, as described above.

332 To better understand these second-order connections, we examined the targets of three
333 classes of regulatory proteins that are prominent amongst Hsp90's clientele: kinases, transcription
334 factors (TFs), and E3 ubiquitin ligases[70]. We first assessed which kinases might connect Hsp90
335 inhibition to changes in the effects of natural variants, identifying seventeen kinases whose
336 targets[38] were enriched for Hsp90-dependent variation (Bonferroni-corrected q value < 0.05) [**Fig.
337 4G, Fig. S4C**] of which thirteen are known to interact with Hsp90[71]. Two of the remaining four
338 interact with either Hsp70 or the kinase adapter Cdc37. Hsp90 exerted a broad influence via these
339 client kinases: ninety-two predicted targets of the client MAP kinase Slt2, for example, bore
340 interacting alleles[72]. The targets of these enriched kinases accounted for another 32.2% of the
341 interacting alleles in our experiments. Indeed, many of these kinases themselves respond to various
342 stresses (*e.g.*, DNA damage and replication checkpoints [Kcc4, Mek1, Rad53, Cdc28, Pcl2],

343 nutrient response [Gcn2, Pho80/Pho85, Rim15]), heat and cold shock and the UPR [Slt2, Kin1],
344 stress granule regulation [Sky1], and osmotic shock [Hog1]), adding another layer of potential
345 environmental specificity.

346 Modified variants were also enriched at the targets of five TFs [**Fig. 4G**, **Fig. S4D**; see
347 **Methods**][39] but comparatively poor characterization of the substrate specificity of E3 ligases[71] [see
348 **Methods**] limited our capacity to assess this class of clients, with only three ligases exhibiting
349 significant enrichments [**Fig. 4G**, **Fig. S4E**][73]. In spite of these limitations, our data establish that
350 > 90% of Hsp90's effects on the inheritance of biological traits can be explained by genetic
351 variation in direct targets of chaperone function or in the targets of kinases, a deeply conserved
352 class of Hsp90 client proteins. This close coupling enables the simultaneous modification of
353 multiple alleles in complex sub-networks engaged by the integration of diverse stress and signaling
354 inputs that control the function of Hsp90 and its client kinases.

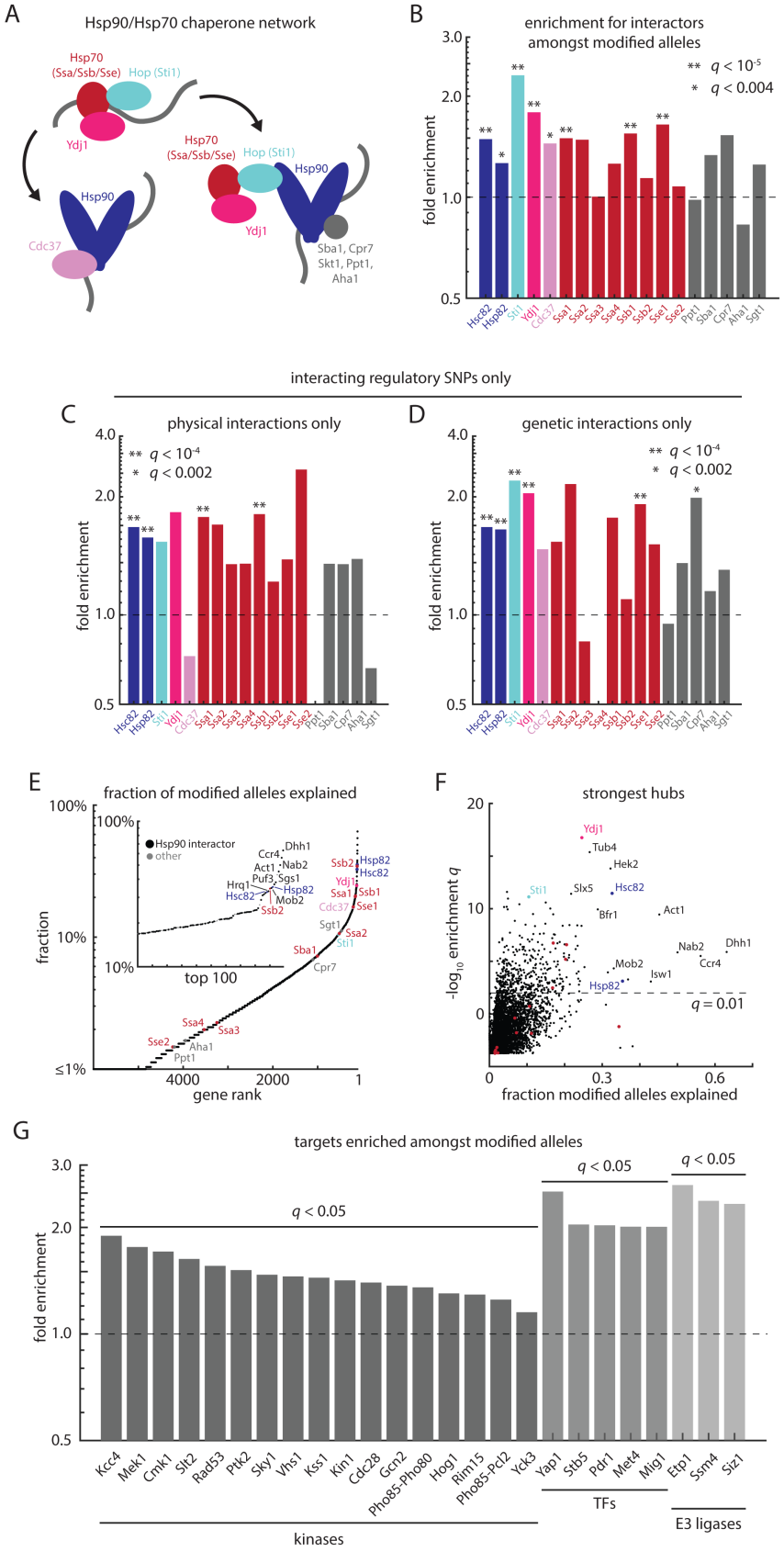
A
Hsp90/Hsp70 chaperone network
Hsp70 (Ssa/Ssb/Sse)
Hop (Sti1)
Ydj1
Hsp90
Cdc37
Sba1, Cpr7 Skt1, Ppt1, Aha1
B
enrichment for interactors amongst modified alleles
** q < 10^-5
* q < 0.004
fold enrichment
interacting regulatory SNPs only
C
physical interactions only
** q < 10^-4
* q < 0.002
D
genetic interactions only
E
fraction of modified alleles explained
Hsp90 interactor
other
top 100
fraction
gene rank
F
strongest hubs
-log10 enrichment q
q = 0.01
fraction modified alleles explained
G
targets enriched amongst modified alleles
q < 0.05
kinases
TFs
E3 ligases

355

356 **Figure 4. Hsp90-dependent phenotypes arise from the Hsp90/Hsp70 chaperone network and**
357 **client regulatory proteins.** (A) Schematic of the Hsp90/Hsp70 chaperone network and associated
358 co-chaperones and adapter proteins[74]. (B) Relative enrichment of interactors of the indicated
359 proteins amongst Hsp90-modified alleles as compared to all segregating genetic variants.
360 Interactions from the BioGRID database. Bonferroni-corrected q values from Fisher's exact test.
361 (C) As in (B), for only regulatory Hsp90-modified variants and physical interactions from
362 BioGRID. (D) As in (B), for only regulatory Hsp90-modified variants and genetic interactions
363 from BioGRID. (E) Genes ranked by the fraction of their interactors amongst Hsp90-modified
364 alleles. Inset: top 100 hits. Chaperone network components are colored as in (A). (F) Interaction
365 enrichment q value (ordinate) as a function of the fraction of interactors amongst Hsp90-modified
366 alleles (abscissa) for all genes in BioGRID. Chaperone network components are colored as in (A).
367 Bonferroni-corrected q values from Fisher's exact test. (G) Relative enrichment of targets of the
368 indicated proteins amongst Hsp90-modified alleles as compared to all segregating genetic variants.
369 Left: kinases; middle: transcription factors; right: E3 ligases. Bonferroni-corrected q values from
370 Fisher's exact test. All proteins shown have $q < 0.05$. See also [**Fig. S4**].

371 ***The influence of Hsp90 on complex heredity***

372 The Hsp90-dependence of phenotype was often highly complex — the median trait comprised 142
373 modified alleles [**Fig. S5A**] – consistent with a widespread reservoir of co-regulated variants under
374 the influence of Hsp90 activity. Hsp90-dependent growth in maltose, for example, depended on
375 three separate large-effect alleles segregating at the *MAL1*, *MAL3*, and *GAL10/GAL1* loci. The
376 modified loci at *MAL3* and *GAL10* included regulatory variants; the locus at *MAL1* mapped to a
377 deletion encompassing three maltose metabolic genes – *IMA1, MAL11*, and *MAL13*[75]. This
378 segmental deletion was much more deleterious to growth in maltose when Hsp90 was inhibited
379 [**Fig. S4B**], indicating that it was buffered by the chaperone. Gal1 is an Hsp90 client, whereas
380 Mal13, Mal33, and Gal10 are clients of Hsp70[36] and the kinase Yck3 is thought to act on Ima1[38],
381 illustrating the far-reaching polygenic impact of the Hsp90 chaperone network.

382 These joint interactions resulted in a remarkably environment-specific effect of Hsp90
383 inhibition on fitness [**Fig. 5A**]. Yet despite Hsp90's pronounced impact in maltose, the three loci
384 had negligible Hsp90 dependence in raffinose [**Fig. 5A**]. This was a general property of Hsp90-
385 dependent heredity in our experiments: the effect of Hsp90 inhibition on the phenotypic
386 consequences of variation was uncorrelated between different stress conditions [**Fig. S5C**]. To
387 better understand how Hsp90 influenced the concerted effects of multiple variants, we examined
388 the eight possible combinations of homozygous genotypes at these three loci and the fitness
389 consequences of evolutionary paths between them. Several of these mutational steps were
390 permitted (did not significantly decrease fitness) exclusively when Hsp90 was either fully active
391 or inhibited [**Fig. S5D**]. This, in turn, altered the mutational paths accessible between genotypes
392 without a stepwise decrease in fitness [**Fig. 5B**]. Simultaneously, Hsp90 inhibition coarsened the
393 landscape: the effect of single-mutation steps[76] in this mutational neighborhood was increased

394 when Hsp90 was inhibited in maltose, but had little effect on the same transitions in raffinose [**Fig.**
395 **5C**]. We observed similar behavior for buffered variants linked to fluconazole resistance at
396 *ERG11*, *PDR1*, and *GRE2* [**Fig. 5DE**], and, as above, these gene products are closely linked to
397 Hsp90 activity: Erg11 is an Hsp90 client, Gre2 a client of Hsp70, and Pdr1 a predicted target of
398 the Rim15, Rad53, Kin1, and Hog1 kinases, among others[36,38]. These results illustrate how Hsp90
399 can affect polygenic adaptation in ways that are highly selective for a given environment. By
400 altering the effects of mutations from deleterious to permissible (neutral), chaperone activity
401 shapes the tradeoff between metabolic specialization and the accessibility of other phenotypes
402 when the environment changes.

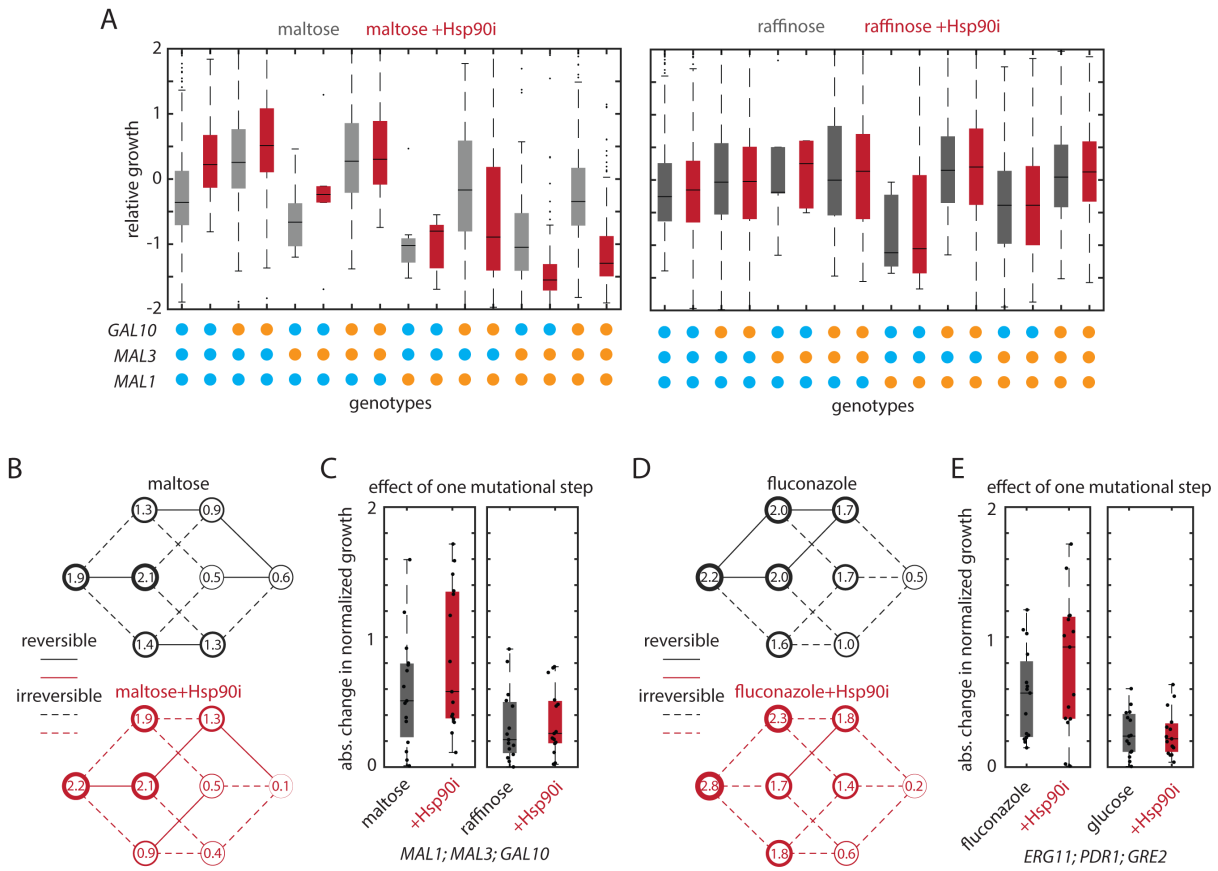

Figure 5. Complex genetic architectures of Hsp90-dependent heredity. (A) Left: Mean normalized growth on maltose of F_6 segregants binned by their genotypes at *GAL10*, *MAL1*, and *MAL3* and organized by their mutational distance from the fittest genotype (*GAL10*^{YJM975}; *MAL1*^{RM11}; *MAL3*^{RM11}) without (black) and with (red; +Hsp90i) inhibition of Hsp90 by radicicol. Box plots show the median and upper and lower quartiles; whiskers show 1.5 times the interquartile range. Right: As left, but for growth in raffinose. (B) Phenotypic landscape of growth in maltose (top) or maltose with radicicol (bottom). Genotypes at *MAL1, MAL3,* and *GAL10* are as indicated in (A); the fitness of each genotype is encoded in the line width of the enclosing circle. Phenotypic landscapes highlight mutational paths accessible by drift (solid lines; reversible; do not significantly decrease fitness; nominal $p > 0.05$) and paths that alter fitness (dashed lines; irreversible; nominal $p < 0.05$). Indicated within each circle is the fitness of that genotype (in units of standard deviations of F_6 growth; adjusted such that fitness values are positive). (C) Change in mean normalized growth on maltose for all possible single-mutation steps amongst *GAL10*, *MAL1*, and *MAL3* alleles with (red) without (black) Hsp90 inhibition by radicicol (+Hsp90i). Box plots show the median and upper and lower quartiles; whiskers show 1.5 times the interquartile range. (D) As in (B), but for *ERG11*, *PDR1*, and *GRE2* in fluconazole and glucose. (E) As in (C), but for *ERG11*, *PDR1*, and *GRE2* in fluconazole and glucose. See also [**Fig. S5**].

421 ***Hsp90-dependent variation at young genes***

422 Our identification of interacting variants not only at the *MAL* but also the *FLO* genes, young,
423 rapidly evolving subtelomeric gene families with highly variable gene content across *S.*
424 *cerevisiae*[77] [**Supplemental File S2**], prompted us to ask if evolutionarily young genes, as a group,
425 were predisposed to harbor Hsp90-dependent variation. After stratifying all *S. cerevisiae* genes by
426 evolutionary age[78] [**Fig. 6A**], we found that the youngest genes harbored alleles that exhibited the
427 strongest Hsp90-dependent phenotypic effects [**Fig. 6B**]. Consistent with the prominent role for
428 *cis*-regulation described above, this enrichment was driven predominantly by regulatory variation
429 [**Fig. 6C**; **Fig. S5E**] and strong buffering interactions [**Fig. S5FG**].

430 In turn, subtelomeric regions across the genome exhibited an unusually high density of
431 Hsp90-dependent mutations relative to their gene content ($p < 10^{-9}$) [**Fig. 6D**]. Indeed, even though
432 the set of natural variants we examined harbors an excess of regulatory mutations near
433 chromosome ends, Hsp90-dependent regulatory variants were nonetheless enriched in these
434 hypervariable regions ($p < 0.03$) [**Fig. S5H**]. Across *S.* cerevisiae, both young and subtelomeric
435 genes are enriched for coding and non-coding polymorphisms [**Fig. 6EF**] Moreover, subtelomeric
436 Hsp90-dependent variants exhibited much stronger buffering interactions as compared to
437 potentiations ($p < 10^{-4}$) than did variants in the remainder of the chromosome **Fig. 6G**]. Thus,
438 Hsp90-buffered variation provides a potent reservoir of phenotypic novelty[79], particularly at
439 subtelomeric genes, such as the *MAL* loci, that are known contribute to niche-specific adaptation
440 and harbor more condition-specific alleles of large effect[77].

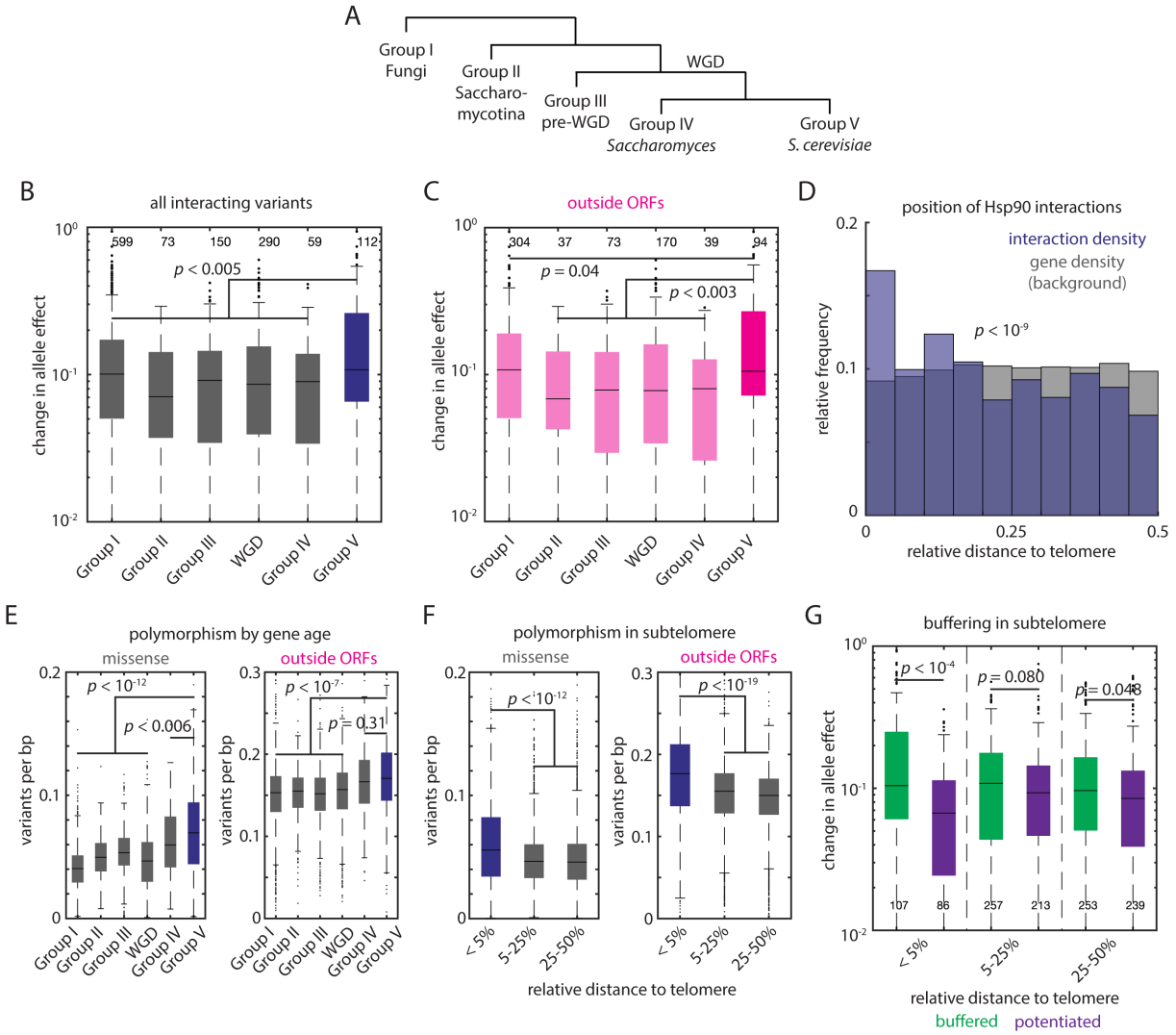

Figure 6. Hsp90 buffers the effects of subtelomeric genetic variation. (A) Schematic of phylogeny used to classify *S. cerevisiae* genes by their evolutionary age based on the presence or absence of homologues in the taxa shown. (B) Absolute change in allele effect for Hsp90-modified variants with ages as indicated. Box plots show the median and upper and lower quartiles; whiskers show 1.5 times the interquartile range; *p* values by Mann-Whitney *U* test. *n* as indicated. (C) As in (B), but only for Hsp90-modified variants outside of open reading frames. (D) Relative frequency of Hsp90-modified variants (blue) and all genes (grey) as a function of distance from the nearest chromosome end (normalized to chromosome length). *p* value by Kolmogorov-Smirnov test. (E) Left: Missense variants per base pair in the 1,002 Yeast Genomes collection for genes with ages as indicated. Right: As left, but for variants outside open reading frames. *p* values by Mann-Whitney *U* test. (F) Left: Missense variants per base pair in the 1,002 Yeast Genomes collection for genes with positions relative to the nearest chromosome end as indicated. Right: As left, but for variants outside open reading frames. *p* values by Mann-Whitney *U* test. (G) Absolute change in allele effect for Hsp90-buffered variants (green) and Hsp90-potentiated variants (purple)

456 with positions relative to the nearest chromosome end as indicated. *p* values by Mann-Whitney *U*
457 test. See also [**Fig. S5**].

458 ***A generalizable model for buffering by Hsp90***

459 How does Hsp90 simultaneously buffer the outcomes of coding and non-coding variation? To
460 investigate this question, we returned to two observations from genetic mapping: first, that Hsp70
461 and Hsp90's direct clients were enriched in interacting genes, and second, that regulatory variation,
462 which does not alter protein sequence, was a central driver of Hsp90-dependent heredity. These
463 observations led us to hypothesize that Hsp90-dependence was often an intrinsic property of
464 certain gene products, rather than a property of particular mutations that led one allele to become
465 Hsp90-dependent.

466 To test this idea, we revisited the buffered *ERG11* regulatory variant [**Fig. 2A**].
467 Interestingly, genetic mapping also suggested a role for the neighboring Erg11^{Asn433Lys} coding
468 variant in azole resistance when Hsp90 was fully active. We hypothesized that, due to a reduction
469 in Erg11 activity upon Hsp90 inhibition, the effects of both variants would be buffered [**Fig. 7A**].
470 After reconstructing sensitive strains bearing each variant singly as well as a strain bearing both
471 mutations, we found that, strikingly, the single and double mutants all exhibited buffered resistance
472 to azoles ($p < 10^{-4}$; $p < 0.001$) [**Fig. 7B**; **Fig. S6A**].

473 We next sought to explain why these distinct mutations were affected similarly by Hsp90.
474 Building on our observation that *cis*-regulatory variation is frequently buffered, we hypothesized
475 that this behavior could arise if activity-to-fitness relationships for a given gene modified by the
476 chaperone were sigmoidal rather than linear [**Fig. 7C**]. Sigmoidal relationships of this kind have
477 been observed empirically for combinations of mutations in proteins[80,81] and for combinations of
478 *cis*-regulatory variants at different genes[82]. Under normal physiological conditions, most such
479 relationships are relatively flat, permitting modestly perturbative variants to accumulate. However,
480 when environmental stress depletes the reservoir of Hsp90 function, sigmoidal activity-to-fitness

481 relationships would be transformed for genes that interact with the chaperone or its client kinases,
482 shifting toward the precipice of a high slope regime. The previously tolerated molecular
483 consequences of variants that cause the protein to be improperly folded, aberrantly post-
484 translationally modified, or decrease its expression would have a very different fitness impact due
485 to the increased local slope of the activity-fitness sigmoid, amplifying the phenotypic impact of
486 buffered variants. Such a model has a striking prediction: for a given locus such as *ERG11,* the
487 fitness effects of arbitrary mutations should depend on Hsp90 activity, and the phenotypic
488 consequences of reducing Erg11 activity should be buffered.

489 To test these predictions quantitatively, we used synthetic CRISPR interference[83] to reduce
490 *ERG11* transcription in the YJM975 parent [**Fig. 7D**]. As compared to a non-targeting guide RNA,
491 reducing *ERG11* levels [**Fig. S6B**] caused a dose-dependent sensitivity to fluconazole [**Fig. 7E**].
492 In turn, Hsp90 inhibition caused a progressively greater sensitivity concomitant with decreasing
493 *ERG11* transcription ($p < 10^{-8}$) [**Fig. 7EF**]. That is, the phenotypic consequences of reduced Erg11
494 activity were systematically buffered by Hsp90, just as we had observed for natural variation.
495 Reducing *ERG11* levels had no effect in the absence of azole, regardless of Hsp90 activity [**Fig.**
496 **S6C**], and comparable results were obtained in the RM11 parent, indicating that the phenomenon
497 was a general property of reduced Erg11 levels rather than a property of a specific *ERG11* genotype
498 [**Fig. S6D**].

499 Finally, we asked whether we could identify genes with a steep activity-fitness relationship
500 that might be more prone to Hsp90-dependent buffering. We examined haploinsufficient genes—
501 those whose heterozygous mutants affect the diploid—because reducing their expression by
502 approximately one-half leads to an appreciable phenotype [**Fig. S6E**]. Indeed, mutations in these
503 genes[84] had stronger Hsp90-dependent effects [**Fig. S6F**]. This did not arise simply because many

504 haploinsufficient genes are essential: essential genes that are not haploinsufficient did not exhibit
505 this trend. Moreover, in concordance with our model, these enrichments arose exclusively amongst
506 buffering interactions [**Fig. 7G**]. Intriguingly, human genes scored as more essential based on the
507 frequency of predicted loss-of-function mutants in gnomAD[85] or identified as haploinsufficient in
508 experiments in embryonic stem cells[86] are also enriched for known Hsp90 interactors[87] [**Fig. 7H**].
509 These genes may likewise be candidates to harbor Hsp90-buffered genetic variation arising from
510 sigmoidal activity-fitness relationships.

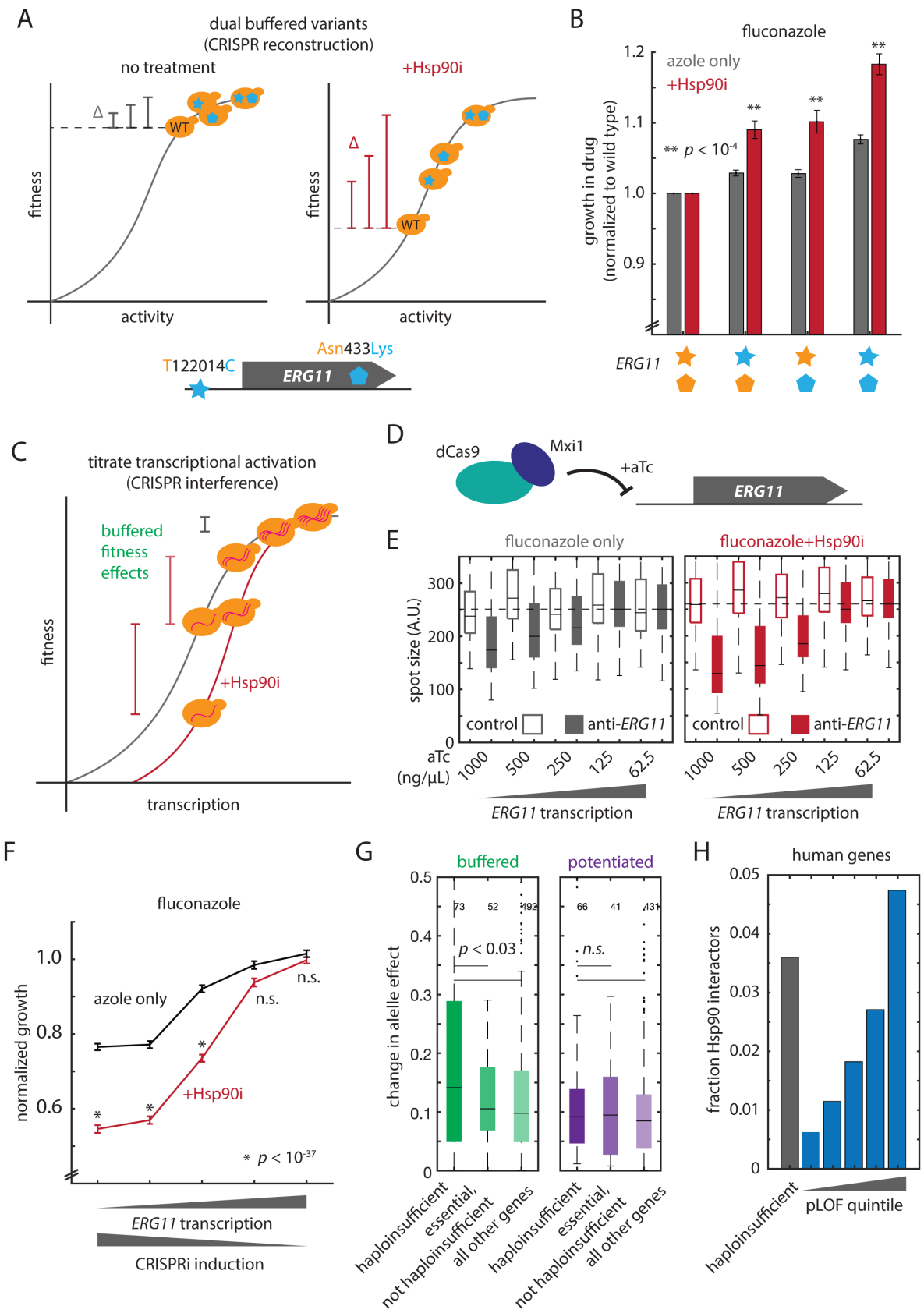
A
dual buffered variants
(CRISPR reconstruction)
no treatment
+Hsp90i
fitness
activity
WT
Δ
T122014C
Asn433Lys
ERG11
B
fluconazole
azole only
+Hsp90i
growth in drug
(normalized to wild type)
** p < 10-4
ERG11
C
titrate transcriptional activation
(CRISPR interference)
buffered
fitness
effects
+Hsp90i
transcription
D
dCas9
Mxi1
+aTc
ERG11
E
fluconazole only
fluconazole+Hsp90i
spot size (A.U.)
control
anti-ERG11
aTc
(ng/μL)
1000
500
250
125
62.5
ERG11 transcription
F
fluconazole
normalized growth
azole only
+Hsp90i
n.s.
* p < 10-37
ERG11 transcription
CRISPRi induction
G
buffered
potentiated
change in alelle effect
p < 0.03
n.s.
haploinsufficient
essential,
not haploinsufficient
all other genes
H
human genes
fraction Hsp90 interactors
pLOF quintile

511

512 **Figure 7: Hsp90 modifies the activity-fitness relationship.** (A) Schematic of the effect of Hsp90
513 inhibition on fitness assuming a non-linear relationship between protein activity and phenotype.
514 Mutations in the hypothetical gene increase activity; the fitness consequences of these changes are
515 amplified when total activity is compromised by Hsp90 inhibition. (B) Growth in fluconazole of
516 genome-edited strains with Hsp90 active (grey) and inhibited with radicicol (+Hsp90i; red). Each
517 panel shows wild type YJM975, edited YJM975 *ERG11*^{122014C}, edited YJM975 Erg11^{433Lys}, and
518 edited double-mutant YJM975 *ERG11*^{122014C} Erg11^{433Lys} strains. Data shown are mean and s.e.m.
519 normalized to the wild type; *p* values by *t* test against the same mutant strain without radicicol
520 treatment; *n* = 384 per genotype. (C) Schematic of the effect of Hsp90 inhibition on fitness
521 assuming a non-linear relationship between protein activity and phenotype. Increasing CRISPRi
522 expression reduces *ERG11* expression; the fitness consequences of these changes are amplified
523 when total activity is compromised by Hsp90 inhibition. (D) Schematic of CRISPR transcriptional
524 interference mediated by a dCas9:Mxi1 fusion and anhydrotetracycline (+aTc) inducible gRNA.
525 (E) Growth of YJM975 haploid strains expressing either a non-targeting control gRNA (open
526 boxes) or an anti-*ERG11* gRNA (closed boxes) in fluconazole without the addition of radicicol
527 (grey boxes) or with radicicol (red boxes). Shown is the concentration of inducing molecule (aTc)
528 added to each culture. Box plots show the median and upper and lower quartiles; whiskers show
529 1.5 times the interquartile range; *n* = 384 per genotype. (F) Data in (E) normalized to the growth
530 of the YJM975 strain expressing the non-targeting control gRNA. Growth is in fluconazole
531 without the addition of radicicol (black) or with radicicol (+Hsp90i; red). The concentrations of
532 inducing molecule (aTc) added to each culture are (left to right) 1000 ng/µL, 500 ng/µL, 250
533 ng/µL, 125 ng/µL, and 62.5 ng/µL. Data shown are mean and s.e.m. (G) Absolute change in allele
534 effect for Hsp90-modified variants in haploinsufficient genes, essential but not haploinsufficient
535 genes, or all other genes, as indicated. Buffered interactions are shown at left (green) and
536 potentiated interactions at right (purple). Box plots show the median and upper and lower quartiles;
537 whiskers show 1.5 times the interquartile range; *p* values by *t* test; *n* as indicated. (H) Fraction of
538 Hsp90-interacting gene products amongst all human genes, divided in quintiles by increasing
539 gnomAD pLOF score (blue) and amongst genes haploinsufficient in embryonic stem cells (grey).
540 See also [**Fig. S6**].

541 **DISCUSSION**

542 The influence of Hsp90 on the developmental and adaptive consequences of genetic variation has
543 long been appreciated. However, aside from a handful of examples of mutations in client proteins,
544 the molecular underpinnings of these effects have remained enigmatic. Here, the unprecedented
545 scale of our nucleotide-resolution approach revealed a surprise: *cis*-regulatory variants, which by
546 definition do not alter protein stability, emerged as a driver of nearly half of Hsp90-dependent
547 phenotypes. This behavior arises naturally from the chaperone's pervasive influence on the
548 activity-fitness relationships of core regulatory proteins. Buffering interactions, which are enriched
549 amongst these relationships, position Hsp90 to govern the release of cryptic, potentially adaptive
550 variation in this regulatory circuitry. This mechanism combines the privileged evolutionary role
551 of *cis*-regulatory variation[88], which enables sophisticated spatiotemporal programming, with the
552 exquisite stress-dependent regulation of the Hsp90 chaperone machinery to release adaptive
553 phenotypes under stress.

554 The preponderance of this behavior in the concise budding yeast genome suggests that
555 interactions between Hsp90 and regulatory variation may be even more prominent in organisms
556 with more elaborate regulatory architectures. Considering the modest number of conditions we
557 surveyed in our experiments, the involvement of more than 10% of genes in Hsp90-dependent
558 phenotypes emphasizes the widespread influence of Hsp90 on heredity. Indeed, the pragmatic need
559 for a low density of polymorphisms in our panel means that our results likely represent a lower
560 bound on the prevalence of this phenomenon, even in budding yeast. Significant technical
561 advances are still needed to understand Hsp90-dependent alleles of small effect and genetic
562 epistasis that is itself controlled by chaperone activity, both of which may play a role in Hsp90-
563 dependent heredity. Nonetheless, even generous estimates of the contribution of epistasis suggest

564 that, for some phenotypic transformations driven by the chaperone, other heritable variation that
565 depends on Hsp90 activity (*e.g.*, prions[89] or long-lived chromatin modifications[6]) may also play
566 an important role.

567 Our experiments identified numerous instances in which the effect of Hsp90 activity on
568 fixed natural polymorphisms was as large as the effect of the variant alone. These were widespread
569 throughout the genome, and although it is not straightforward to infer selection coefficients
570 directly from genetic mapping experiments, the effects we observed likely exceed the threshold
571 for effective selection by multiple orders of magnitude. That many Hsp90-contingent effects were
572 buffered and highly condition-specific further suggests a role in adaptation. Connecting a wide
573 array of mutations to chaperone activity both directly and *via* client regulatory proteins may confer
574 a particular advantage in rapidly changing environments[90], when modular regulons can be engaged
575 in a stress-dependent fashion (*e.g.* by kinases).

576 Indeed, multiple mechanisms may converge on a single protein: many interacting alleles
577 at direct clients were also *trans* targets of client regulators. The environmental specificity of these
578 interactions means that buffered variation can accumulate under normal conditions without
579 compromising fitness. At the same time, this variation is likely shaped by repeated selection during
580 periods when Hsp90 activity is compromised. This allows a greater diversity of genetic variation
581 to persist in the population[91], broadening the accessible adaptive trajectories under stress.
582 Moreover, by virtue of repeated cycles of selection, this reservoir of genetic potential may be
583 predisposed to drive adaptive phenotypes[92]. Our results also explain why Hsp90 has such a
584 profound impact on development, where the revelation of phenotypes due to *cis*-acting regulation
585 would have especially potent consequences.

586 Might there be an advantage to maintaining such a dependence on Hsp90? Some
587 connections may be an inevitable consequence of kinase structure and dynamics, although the
588 diversity of client status within kinases families suggests that these proteins can readily evolve
589 away from chaperone dependence[8]. Our results illustrate a potential evolutionary advantage for
590 the retention of this dependence. Sigmoidal activity-to-fitness relationships, which are common
591 among Hsp90 clients, limit the fitness effects of modest perturbations to a protein's activity. Yet
592 they also amplify the phenotypic consequences of variants that spark larger excursions in activity.
593 Coupling Hsp90 function to the shape of such activity-to-fitness relationships thus provides a route
594 for organisms to reconcile the competing evolutionary demands of robustness and evolvability by
595 modulating the fitness consequences of changes in activity in response to environmental
596 conditions.

597 The mechanisms we have discovered allow the evolutionary potential of variants of large
598 effect to be harnessed precisely when organisms are most ill-suited to their environments. The
599 involvement of highly polymorphic subtelomeric genes may enhance this phenomenon, as may
600 other environmentally responsive mechanisms, such as the Hsp90-dependent [*ESI*$^{+}$] prion. This
601 epigenetic element regulates the expression of previously silent genetic information in precisely
602 these regions[93]. In some instances, Hsp90 contingency may even be co-opted as a regulatory
603 strategy. Haploinsufficient genes, which are enriched in Hsp90 clients, may preferentially harbor
604 such buffered *cis*-regulatory effects, and our data suggest *cis*-regulatory variants controlling
605 proteins known to interact with Hsp90 or its client kinases may be especially profitable to explore.
606 Understanding how the integration of Hsp90 and kinase signaling modules enable re-interpretation
607 of the genotype-to-phenotype relationship in different environmental contexts is also an exciting
608 avenue for future discovery.

609 Prior studies have indicated that Hsp90 facilitates the accumulation of coding variation in
610 clients[94], accelerating their evolution[95]. Our findings suggest that the chaperone enables the
611 accumulation of cryptic regulatory variation at these genes at least as strongly, which provides an
612 unappreciated and appealing potential mechanism for the influence of Hsp90 on developmental
613 evolution in diverse systems from fruit flies to Mexican cavefish. Likewise, in cancer and in
614 pathogens, the buffering of drug-resistant regulatory mutations by Hsp90 may allow their
615 accumulation, subsequently being enriched amongst the surviving cells following treatment and
616 promoting future drug-resistance. This, in turn, suggests that a paradigm favoring therapeutic
617 Hsp90 inhibition, predicated on the Hsp90-addicted v-Src kinase, may be counterproductive if
618 cryptic, buffered resistance is revealed and enriched. Distinguishing cases in which Hsp90
619 inhibition is helpful or deleterious to treatment is an important question for future investigation, as
620 is the relationship between an individual's reservoir of Hsp90-dependent buffering capacity and
621 their polygenic risk for genetic disease. The decline of this buffering reservoir throughout the
622 lifespan may also contribute to the emergence of pathologies with age.

623 Our findings address long-standing mechanistic questions surrounding the role of Hsp90
624 in transmuting genetic variation into selectable phenotypes. Hsp90's activity and connectivity with
625 an expansive regulon of client proteins position it to control activity-fitness relationships, and their
626 evolution, throughout the core eukaryotic regulatory circuitry. In turn, the effects of numerous
627 coding and regulatory variants simultaneously depend strongly on its stress-regulated activity.
628 Finally, the acute environmental specificity of these buffered fitness effects facilitates their
629 accumulation in advance of stress. Together, these features render Hsp90 a central governor of the
630 critical evolutionary tradeoff between robustness and adaptability in the face of a changing
631 environment, when diversification is most crucial.

632 **REFERENCES**

633 1. Cooper, D.N., Krawczak, M., Polychronakos, C., Tyler-Smith, C., and Kehrer-Sawatzki, H. (2013).
634 Where genotype is not predictive of phenotype: towards an understanding of the molecular basis of
635 reduced penetrance in human inherited disease. Hum. Genet. *132*, 1077–1130.
636 https://doi.org/10.1007/s00439-013-1331-2.

637 2. Jablonka, E., and Lamb, M.J. (1998). Epigenetic inheritance in evolution. J. Evol. Biol. *11*, 159–183.
638 https://doi.org/10.1046/j.1420-9101.1998.11020159.x.

639 3. Gee, Henry, Howlett, R., and Campbell, P. (2009). 15 Evolutionary Gems. Nature.
640 https://doi.org/10.1038/nature07740.

641 4. Bergman, A., and Siegal, M.L. (2003). Evolutionary capacitance as a general feature of complex gene
642 networks. Nature *424*, 549–552. https://doi.org/10.1038/nature01765.

643 5. Borkovich, K.A., Farrelly, F.W., Finkelstein, D.B., Taulien, J., and Lindquist, S. (1989). hsp82 is an
644 essential protein that is required in higher concentrations for growth of cells at higher temperatures.
645 Mol. Cell. Biol. *9*, 3919–3930. https://doi.org/10.1128/MCB.9.9.3919.

646 6. Sawarkar, R., and Paro, R. (2013). Hsp90@chromatin.nucleus: an emerging hub of a networker.
647 Trends Cell Biol. *23*, 193–201. https://doi.org/10.1016/j.tcb.2012.11.007.

648 7. Gopinath, R.K., You, S.-T., Chien, K.-Y., Swamy, K.B.S., Yu, J.-S., Schuyler, S.C., and Leu, J.-Y.
649 (2014). The Hsp90-Dependent Proteome Is Conserved and Enriched for Hub Proteins with High
650 Levels of Protein–Protein Connectivity. Genome Biol. Evol. *6*, 2851–2865.
651 https://doi.org/10.1093/gbe/evu226.

652 8. Taipale, M., Krykbaeva, I., Koeva, M., Kayatekin, C., Westover, K.D., Karras, G.I., and Lindquist, S.
653 (2012). Quantitative analysis of HSP90-client interactions reveals principles of substrate
654 recognition. Cell *150*, 987–1001. https://doi.org/10.1016/j.cell.2012.06.047.

655 9. Csermely, P., Schnaider, T., So″ti, C., Prohászka, Z., and Nardai, G. (1998). The 90-kDa Molecular
656 Chaperone Family: Structure, Function, and Clinical Applications. A Comprehensive Review.
657 Pharmacol. Ther. *79*, 129–168. https://doi.org/10.1016/S0163-7258(98)00013-8.

658 10. Picard, D., Khursheed, B., Garabedian, M.J., Fortin, M.G., Lindquist, S., and Yamamoto, K.R.
659 (1990). Reduced levels of hsp90 compromise steroid receptor action in vivo. Nature *348*, 166–168.
660 https://doi.org/10.1038/348166a0.

661 11. Rohner, N., Jarosz, D.F., Kowalko, J.E., Yoshizawa, M., Jeffery, W.R., Borowsky, R.L., Lindquist,
662 S., and Tabin, C.J. (2013). Cryptic Variation in Morphological Evolution: HSP90 as a Capacitor for
663 Loss of Eyes in Cavefish. Science *342*, 1372–1375. https://doi.org/10.1126/science.1240276.

664 12. Cowen, L.E., and Lindquist, S. (2005). Hsp90 Potentiates the Rapid Evolution of New Traits: Drug
665 Resistance in Diverse Fungi. Science *309*, 2185–2189. https://doi.org/10.1126/science.1118370.

666 13. Geiler-Samerotte, K.A., Zhu, Y.O., Goulet, B.E., Hall, D.W., and Siegal, M.L. (2016). Selection
667 Transforms the Landscape of Genetic Variation Interacting with Hsp90. PLOS Biol. *14*, e2000465.
668 https://doi.org/10.1371/journal.pbio.2000465.

669 14. Karras, G.I., Yi, S., Sahni, N., Fischer, M., Xie, J., Vidal, M., D'Andrea, A.D., Whitesell, L., and
670 Lindquist, S. (2017). HSP90 Shapes the Consequences of Human Genetic Variation. Cell *168*, 856-
671 866.e12. https://doi.org/10.1016/j.cell.2017.01.023.

672 15. Queitsch, C., Sangster, T.A., and Lindquist, S. (2002). Hsp90 as a capacitor of phenotypic variation.
673 Nature *417*, 618–624. https://doi.org/10.1038/nature749.

674 16. Rutherford, S.L., and Lindquist, S. (1998). Hsp90 as a capacitor for morphological evolution. Nature
675 *396*, 336–342. https://doi.org/10.1038/24550.

676 17. Sangster, T.A., Salathia, N., Lee, H.N., Watanabe, E., Schellenberg, K., Morneau, K., Wang, H.,
677 Undurraga, S., Queitsch, C., and Lindquist, S. (2008). HSP90-buffered genetic variation is common
678 in Arabidopsis thaliana. Proc. Natl. Acad. Sci. *105*, 2969–2974.
679 https://doi.org/10.1073/pnas.0712210105.

680 18. Xu, Y., Singer, M.A., and Lindquist, S. (1999). Maturation of the tyrosine kinase c-src as a kinase
681 and as a substrate depends on the molecular chaperone Hsp90. Proc. Natl. Acad. Sci. *96*, 109–114.
682 https://doi.org/10.1073/pnas.96.1.109.

683 19. Whitesell, L., and Lindquist, S.L. (2005). HSP90 and the chaperoning of cancer. Nat. Rev. Cancer *5*,
684 761–772. https://doi.org/10.1038/nrc1716.

685 20. Jaeger, A.M., and Whitesell, L. (2019). HSP90: Enabler of Cancer Adaptation. Annu. Rev. Cancer
686 Biol. *3*, 275–297. https://doi.org/10.1146/annurev-cancerbio-030518-055533.

687 21. Luo, W., Sun, W., Taldone, T., Rodina, A., and Chiosis, G. (2010). Heat shock protein 90 in
688 neurodegenerative diseases. Mol. Neurodegener. *5*, 24. https://doi.org/10.1186/1750-1326-5-24.

689 22. Chen, B., and Wagner, A. (2012). Hsp90 is important for fecundity, longevity, and buffering of
690 cryptic deleterious variation in wild fly populations. BMC Evol. Biol. *12*, 25.
691 https://doi.org/10.1186/1471-2148-12-25.

692 23. Condic, N., Amiji, H., Patel, D., Shropshire, W.C., Lermi, N.O., Sabha, Y., John, B., Hanson, B., and
693 Karras, G.I. (2024). Selection for robust metabolism in domesticated yeasts is driven by adaptation
694 to Hsp90 stress. Science *385*, eadi3048. https://doi.org/10.1126/science.adi3048.

695 24. Costanzo, M., VanderSluis, B., Koch, E.N., Baryshnikova, A., Pons, C., Tan, G., Wang, W., Usaj,
696 M., Hanchard, J., Lee, S.D., et al. (2016). A global genetic interaction network maps a wiring
697 diagram of cellular function. Science *353*, aaf1420. https://doi.org/10.1126/science.aaf1420.

698 25. McClellan, A.J., Xia, Y., Deutschbauer, A.M., Davis, R.W., Gerstein, M., and Frydman, J. (2007).
699 Diverse Cellular Functions of the Hsp90 Molecular Chaperone Uncovered Using Systems
700 Approaches. Cell *131*, 121–135. https://doi.org/10.1016/j.cell.2007.07.036.

701 26. Jarosz, D.F., and Lindquist, S. (2010). Hsp90 and Environmental Stress Transform the Adaptive
702 Value of Natural Genetic Variation. Science *330*, 1820–1824.
703 https://doi.org/10.1126/science.1195487.

704 27. Sahni, N., Yi, S., Taipale, M., Fuxman Bass, J.I., Coulombe-Huntington, J., Yang, F., Peng, J., Weile,
705 J., Karras, G.I., Wang, Y., et al. (2015). Widespread Macromolecular Interaction Perturbations in
706 Human Genetic Disorders. Cell *161*, 647–660. https://doi.org/10.1016/j.cell.2015.04.013.

707 28. Prud'homme, B., Gompel, N., and Carroll, S.B. (2007). Emerging principles of regulatory evolution.
708 Proc. Natl. Acad. Sci. *104*, 8605–8612. https://doi.org/10.1073/pnas.0700488104.

709 29. Schopf, F.H., Biebl, M.M., and Buchner, J. (2017). The HSP90 chaperone machinery. Nat. Rev. Mol.
710 Cell Biol. *18*, 345–360. https://doi.org/10.1038/nrm.2017.20.

711 30. Jakobson, C.M., and Jarosz, D.F. (2019). Molecular Origins of Complex Heritability in Natural
712 Genotype-to-Phenotype Relationships. Cell Syst. *8*, 363-379.e3.
713 https://doi.org/10.1016/j.cels.2019.04.002.

714 31. She, R., and Jarosz, D.F. (2018). Mapping Causal Variants with Single-Nucleotide Resolution
715 Reveals Biochemical Drivers of Phenotypic Change. Cell *172*, 478-490.e15.
716 https://doi.org/10.1016/j.cell.2017.12.015.

717 32. Liti, G., Carter, D.M., Moses, A.M., Warringer, J., Parts, L., James, S.A., Davey, R.P., Roberts, I.N.,
718 Burt, A., Koufopanou, V., et al. (2009). Population genomics of domestic and wild yeasts. Nature
719 *458*, 337–341. https://doi.org/10.1038/nature07743.

720 33. Peter, J., Chiara, M.D., Friedrich, A., Yue, J.-X., Pflieger, D., Bergström, A., Sigwalt, A., Barre, B.,
721 Freel, K., Llored, A., et al. (2018). Genome evolution across 1,011 Saccharomyces cerevisiae
722 isolates. Nature, 1. https://doi.org/10.1038/s41586-018-0030-5.

723 34. Giaever, G., Chu, A.M., Ni, L., Connelly, C., Riles, L., Véronneau, S., Dow, S., Lucau-Danila, A.,
724 Anderson, K., André, B., et al. (2002). Functional profiling of the Saccharomyces cerevisiae
725 genome. Nature *418*, 387–391. https://doi.org/10.1038/nature00935.

726 35. Sharon, E., Chen, S.-A.A., Khosla, N.M., Smith, J.D., Pritchard, J.K., and Fraser, H.B. (2018).
727 Functional Genetic Variants Revealed by Massively Parallel Precise Genome Editing. Cell.
728 https://doi.org/10.1016/j.cell.2018.08.057.

729 36. Gong, Y., Kakihara, Y., Krogan, N., Greenblatt, J., Emili, A., Zhang, Z., and Houry, W.A. (2009).
730 An atlas of chaperone–protein interactions in Saccharomyces cerevisiae: implications to protein
731 folding pathways in the cell. Mol. Syst. Biol. *5*, 275. https://doi.org/10.1038/msb.2009.26.

732 37. Girstmair, H., Tippel, F., Lopez, A., Tych, K., Stein, F., Haberkant, P., Schmid, P.W.N., Helm, D.,
733 Rief, M., Sattler, M., et al. (2019). The Hsp90 isoforms from S. cerevisiae differ in structure,
734 function and client range. Nat. Commun. *10*, 3626. https://doi.org/10.1038/s41467-019-11518-w.

735 38. Mok, J., Kim, P.M., Lam, H.Y.K., Piccirillo, S., Zhou, X., Jeschke, G.R., Sheridan, D.L., Parker,
736 S.A., Desai, V., Jwa, M., et al. (2010). Deciphering protein kinase specificity through large-scale
737 analysis of yeast phosphorylation site motifs. Sci. Signal. *3*, ra12.
738 https://doi.org/10.1126/scisignal.2000482.

739 39. Rossi, M.J., Kuntala, P.K., Lai, W.K.M., Yamada, N., Badjatia, N., Mittal, C., Kuzu, G., Bocklund,
740 K., Farrell, N.P., Blanda, T.R., et al. (2021). A high-resolution protein architecture of the budding
741 yeast genome. Nature *592*, 309–314. https://doi.org/10.1038/s41586-021-03314-8.

742 40. Messner, C.B., Demichev, V., Muenzner, J., Aulakh, S.K., Barthel, N., Röhl, A., Herrera-
743 Domínguez, L., Egger, A.-S., Kamrad, S., Hou, J., et al. (2023). The proteomic landscape of
744 genome-wide genetic perturbations. Cell *186*, 2018-2034.e21.
745 https://doi.org/10.1016/j.cell.2023.03.026.

746 41. Jakobson, C.M., She, R., and Jarosz, D.F. (2019). Pervasive function and evidence for selection
747 across standing genetic variation in S. cerevisiae. Nat. Commun. *10*, 1222.
748 https://doi.org/10.1038/s41467-019-09166-1.

749 42. Török, T., Mortimer, R.K., Romano, P., Suzzi, G., and Polsinelli, M. (1996). Quest for wine yeasts—
750 An old story revisited. J. Ind. Microbiol. *17*, 303–313. https://doi.org/10.1007/BF01574705.

751 43. McCullough, M.J., Clemons, K.V., Farina, C., McCusker, J.H., and Stevens, D.A. (1998).
752 Epidemiological investigation of vaginal Saccharomyces cerevisiae isolates by a genotypic method.
753 J. Clin. Microbiol. *36*, 557–562.

754 44. Sharma, S.V., Agatsuma, T., and Nakano, H. (1998). Targeting of the protein chaperone, HSP90, by
755 the transformation suppressing agent, radicicol. Oncogene *16*, 2639–2645.
756 https://doi.org/10.1038/sj.onc.1201790.

757 45. Sarbassov, D.D., Ali, S.M., Kim, D.-H., Guertin, D.A., Latek, R.R., Erdjument-Bromage, H.,
758 Tempst, P., and Sabatini, D.M. (2004). Rictor, a novel binding partner of mTOR, defines a
759 rapamycin-insensitive and raptor-independent pathway that regulates the cytoskeleton. Curr. Biol.
760 CB *14*, 1296–1302. https://doi.org/10.1016/j.cub.2004.06.054.

761 46. Gibson, G. (2009). Decanalization and the origin of complex disease. Nat. Rev. Genet. *10*, 134–140.
762 https://doi.org/10.1038/nrg2502.

763 47. Paaby, A.B., and Rockman, M.V. (2014). Cryptic genetic variation, evolution's hidden substrate. Nat.
764 Rev. Genet. *15*, 247–258. https://doi.org/10.1038/nrg3688.

765 48. Greig, D., and Leu, J.-Y. (2009). Natural history of budding yeast. Curr. Biol. *19*, R886–R890.
766 https://doi.org/10.1016/j.cub.2009.07.037.

767 49. Ho, P.-W., Piampongsant, S., Gallone, B., Del Cortona, A., Peeters, P.-J., Reijbroek, F., Verbaet, J.,
768 Herrera, B., Cortebeeck, J., Nolmans, R., et al. (2021). Massive QTL analysis identifies pleiotropic
769 genetic determinants for stress resistance, aroma formation, and ethanol, glycerol and isobutanol
770 production in Saccharomyces cerevisiae. Biotechnol. Biofuels *14*, 211.
771 https://doi.org/10.1186/s13068-021-02059-w.

772 50. Loewith, R., Jacinto, E., Wullschleger, S., Lorberg, A., Crespo, J.L., Bonenfant, D., Oppliger, W.,
773 Jenoe, P., and Hall, M.N. (2002). Two TOR Complexes, Only One of which Is Rapamycin
774 Sensitive, Have Distinct Roles in Cell Growth Control. Mol. Cell *10*, 457–468.
775 https://doi.org/10.1016/S1097-2765(02)00636-6.

776 51. Jumper, J., Evans, R., Pritzel, A., Green, T., Figurnov, M., Ronneberger, O., Tunyasuvunakool, K.,
777 Bates, R., Žídek, A., Potapenko, A., et al. (2021). Highly accurate protein structure prediction with
778 AlphaFold. Nature *596*, 583–589. https://doi.org/10.1038/s41586-021-03819-2.

779 52. Gaubitz, C., Oliveira, T.M., Prouteau, M., Leitner, A., Karuppasamy, M., Konstantinidou, G., Rispal,
780 D., Eltschinger, S., Robinson, G.C., Thore, S., et al. (2015). Molecular Basis of the Rapamycin
781 Insensitivity of Target Of Rapamycin Complex 2. Mol. Cell *58*, 977–988.
782 https://doi.org/10.1016/j.molcel.2015.04.031.

783 53. Whitesell, L., Mimnaugh, E.G., De Costa, B., Myers, C.E., and Neckers, L.M. (1994). Inhibition of
784 heat shock protein HSP90-pp60v-src heteroprotein complex formation by benzoquinone

785 ansamycins: essential role for stress proteins in oncogenic transformation. Proc. Natl. Acad. Sci. U.
786 S. A. *91*, 8324–8328. https://doi.org/10.1073/pnas.91.18.8324.

787 54. Karst, F., and Lacroute, F. (1977). Ergosterol biosynthesis inSaccharomyces cerevisiae. Mol. Gen.
788 Genet. MGG *154*, 269–277. https://doi.org/10.1007/BF00571282.

789 55. Müller, F.-M.C., Staudigel, A., Salvenmoser, S., Tredup, A., Miltenberger, R., and Herrmann, J.V.
790 (2007). Cross-Resistance to Medical and Agricultural Azole Drugs in Yeasts from the Oropharynx
791 of Human Immunodeficiency Virus Patients and from Environmental Bavarian Vine Grapes.
792 Antimicrob. Agents Chemother. *51*, 3014–3016. https://doi.org/10.1128/aac.00459-07.

793 56. Fisher, M.C., Alastruey-Izquierdo, A., Berman, J., Bicanic, T., Bignell, E.M., Bowyer, P., Bromley,
794 M., Brüggemann, R., Garber, G., Cornely, O.A., et al. (2022). Tackling the emerging threat of
795 antifungal resistance to human health. Nat. Rev. Microbiol. *20*, 557–571.
796 https://doi.org/10.1038/s41579-022-00720-1.

797 57. Yan, H., Yuan, W., Velculescu, V.E., Vogelstein, B., and Kinzler, K.W. (2002). Allelic Variation in
798 Human Gene Expression. Science *297*, 1143–1143. https://doi.org/10.1126/science.1072545.

799 58. Gera, T., Jonas, F., More, R., and Barkai, N. (2022). Evolution of binding preferences among whole-
800 genome duplicated transcription factors. eLife *11*, e73225. https://doi.org/10.7554/eLife.73225.

801 59. Tan, L., Chen, L., Yang, H., Jin, B., Kim, G., and Im, Y.J. (2022). Structural basis for activation of
802 fungal sterol receptor Upc2 and azole resistance. Nat. Chem. Biol. *18*, 1253–1262.
803 https://doi.org/10.1038/s41589-022-01117-0.

804 60. Xia, X. (2019). Translation Control of HAC1 by Regulation of Splicing in Saccharomyces cerevisiae.
805 Int. J. Mol. Sci. *20*, 2860. https://doi.org/10.3390/ijms20122860.

806 61. Aragón, T., van Anken, E., Pincus, D., Serafimova, I.M., Korennykh, A.V., Rubio, C.A., and Walter,
807 P. (2009). mRNA Targeting to ER Stress Signaling Sites. Nature *457*, 736–740.
808 https://doi.org/10.1038/nature07641.

809 62. Freeberg, M.A., Han, T., Moresco, J.J., Kong, A., Yang, Y.-C., Lu, Z.J., Yates, J.R., and Kim, J.K.
810 (2013). Pervasive and dynamic protein binding sites of the mRNA transcriptome in Saccharomyces
811 cerevisiae. Genome Biol. *14*, R13. https://doi.org/10.1186/gb-2013-14-2-r13.

812 63. Pechmann, S., and Frydman, J. (2013). Evolutionary conservation of codon optimality reveals hidden
813 signatures of cotranslational folding. Nat. Struct. Mol. Biol. *20*, 237–243.
814 https://doi.org/10.1038/nsmb.2466.

815 64. Sharma, A.K., Venezian, J., Shiber, A., Kramer, G., Bukau, B., and O'Brien, E.P. (2021).
816 Combinations of slow-translating codon clusters can increase mRNA half-life in Saccharomyces
817 cerevisiae. Proc. Natl. Acad. Sci. *118*, e2026362118. https://doi.org/10.1073/pnas.2026362118.

818 65. Metzl-Raz, E., Kafri, M., Yaakov, G., Soifer, I., Gurvich, Y., and Barkai, N. (2017). Principles of
819 cellular resource allocation revealed by condition-dependent proteome profiling. eLife *6*, e28034.
820 https://doi.org/10.7554/eLife.28034.

821 66. Oughtred, R., Rust, J., Chang, C., Breitkreutz, B.-J., Stark, C., Willems, A., Boucher, L., Leung, G.,
822 Kolas, N., Zhang, F., et al. (2021). The BioGRID database: A comprehensive biomedical resource

823 of curated protein, genetic, and chemical interactions. Protein Sci. Publ. Protein Soc. *30*, 187–200.
824 https://doi.org/10.1002/pro.3978.

825 67. Genest, O., Wickner, S., and Doyle, S.M. (2019). Hsp90 and Hsp70 chaperones: Collaborators in
826 protein remodeling. J. Biol. Chem. *294*, 2109–2120. https://doi.org/10.1074/jbc.REV118.002806.

827 68. Wegele, H., Wandinger, S.K., Schmid, A.B., Reinstein, J., and Buchner, J. (2006). Substrate transfer
828 from the chaperone Hsp70 to Hsp90. J. Mol. Biol. *356*, 802–811.
829 https://doi.org/10.1016/j.jmb.2005.12.008.

830 69. Wang, R.Y.-R., Noddings, C.M., Kirschke, E., Myasnikov, A.G., Johnson, J.L., and Agard, D.A.
831 (2022). Structure of Hsp90-Hsp70-Hop-GR reveals the Hsp90 client-loading mechanism. Nature
832 *601*, 460–464. https://doi.org/10.1038/s41586-021-04252-1.

833 70. Taipale, M., Jarosz, D.F., and Lindquist, S. (2010). HSP90 at the hub of protein homeostasis:
834 emerging mechanistic insights. Nat. Rev. Mol. Cell Biol. *11*, 515–528.
835 https://doi.org/10.1038/nrm2918.

836 71. Cherry, J.M., Hong, E.L., Amundsen, C., Balakrishnan, R., Binkley, G., Chan, E.T., Christie, K.R.,
837 Costanzo, M.C., Dwight, S.S., Engel, S.R., et al. (2012). Saccharomyces Genome Database: the
838 genomics resource of budding yeast. Nucleic Acids Res. *40*, D700–D705.
839 https://doi.org/10.1093/nar/gkr1029.

840 72. Millson, S.H., Truman, A.W., and Piper, P.W. (2022). Hsp90 and phosphorylation of the Slt2(Mpk1)
841 MAP kinase activation loop are essential for catalytic, but not non-catalytic, Slt2-mediated
842 transcription in yeast. Cell Stress Chaperones *27*, 295–304. https://doi.org/10.1007/s12192-022-
843 01274-0.

844 73. Iconomou, M., and Saunders, D.N. (2016). Systematic approaches to identify E3 ligase substrates.
845 Biochem. J. *473*, 4083–4101. https://doi.org/10.1042/BCJ20160719.

846 74. Verghese, J., Abrams, J., Wang, Y., and Morano, K.A. (2012). Biology of the Heat Shock Response
847 and Protein Chaperones: Budding Yeast (Saccharomyces cerevisiae) as a Model System. Microbiol
848 Mol Biol Rev *76*, 115–158. https://doi.org/10.1128/MMBR.05018-11.

849 75. Cohen, J.D., Goldenthal, M.J., Buchferer, B., and Marmur, J. (1984). Mutational analysis of the
850 MAL1 locus of Saccharomyces: identification and functional characterization of three genes. Mol.
851 Gen. Genet. MGG *196*, 208–216. https://doi.org/10.1007/BF00328052.

852 76. Poelwijk, F.J., Socolich, M., and Ranganathan, R. (2019). Learning the pattern of epistasis linking
853 genotype and phenotype in a protein. Nat. Commun. *10*, 4213. https://doi.org/10.1038/s41467-019-
854 12130-8.

855 77. Snoek, T., Voordeckers, K., and Verstrepen, K.J. (2014). Subtelomeric Regions Promote
856 Evolutionary Innovation of Gene Families in Yeast. In Subtelomeres (Springer, Berlin, Heidelberg),
857 pp. 39–70. https://doi.org/10.1007/978-3-642-41566-1_3.

858 78. Doughty, T.W., Domenzain, I., Millan-Oropeza, A., Montini, N., de Groot, P.A., Pereira, R., Nielsen,
859 J., Henry, C., Daran, J.-M.G., Siewers, V., et al. (2020). Stress-induced expression is enriched for
860 evolutionarily young genes in diverse budding yeasts. Nat. Commun. *11*, 2144.
861 https://doi.org/10.1038/s41467-020-16073-3.

862 79. Pál, C., and Papp, B. (2017). Evolution of complex adaptations in molecular systems. Nat. Ecol.
863 Evol. *1*, 1084. https://doi.org/10.1038/s41559-017-0228-1.

864 80. Domingo, J., Baeza-Centurion, P., and Lehner, B. (2019). The Causes and Consequences of Genetic
865 Interactions (Epistasis). Annu. Rev. Genomics Hum. Genet. *20*, 433–460.
866 https://doi.org/10.1146/annurev-genom-083118-014857.

867 81. Jakobson, C.M., and Jarosz, D.F. (2020). What Has a Century of Quantitative Genetics Taught Us
868 About Nature's Genetic Toolkit? Annu. Rev. Genet. *54*, 19.1-19.26.
869 https://doi.org/10.1146/annurev-genet-021920-102037.

870 82. Aguirre, L., Hendelman, A., Hutton, S.F., McCandlish, D.M., and Lippman, Z.B. (2023).
871 Idiosyncratic and dose-dependent epistasis drives variation in tomato fruit size. Science *382*, 315–
872 320. https://doi.org/10.1126/science.adi5222.

873 83. Smith, J.D., Suresh, S., Schlecht, U., Wu, M., Wagih, O., Peltz, G., Davis, R.W., Steinmetz, L.M.,
874 Parts, L., and St.Onge, R.P. (2016). Quantitative CRISPR interference screens in yeast identify
875 chemical-genetic interactions and new rules for guide RNA design. Genome Biol. *17*, 45.
876 https://doi.org/10.1186/s13059-016-0900-9.

877 84. Ohnuki, S., and Ohya, Y. (2018). High-dimensional single-cell phenotyping reveals extensive
878 haploinsufficiency. PLOS Biol. *16*, e2005130. https://doi.org/10.1371/journal.pbio.2005130.

879 85. Karczewski, K.J., Francioli, L.C., Tiao, G., Cummings, B.B., Alföldi, J., Wang, Q., Collins, R.L.,
880 Laricchia, K.M., Ganna, A., Birnbaum, D.P., et al. (2020). The mutational constraint spectrum
881 quantified from variation in 141,456 humans. Nature *581*, 434–443. https://doi.org/10.1038/s41586-
882 020-2308-7.

883 86. Sarel-Gallily, R., Golan-Lev, T., Yilmaz, A., Sagi, I., and Benvenisty, N. (2022). Genome-wide
884 analysis of haploinsufficiency in human embryonic stem cells. Cell Rep. *38*, 110573.
885 https://doi.org/10.1016/j.celrep.2022.110573.

886 87. Echeverría, P.C., Bernthaler, A., Dupuis, P., Mayer, B., and Picard, D. (2011). An Interaction
887 Network Predicted from Public Data as a Discovery Tool: Application to the Hsp90 Molecular
888 Chaperone Machine. PLOS ONE *6*, e26044. https://doi.org/10.1371/journal.pone.0026044.

889 88. Gasch, A.P., Moses, A.M., Chiang, D.Y., Fraser, H.B., Berardini, M., and Eisen, M.B. (2004).
890 Conservation and Evolution of Cis-Regulatory Systems in Ascomycete Fungi. PLOS Biol. *2*, e398.
891 https://doi.org/10.1371/journal.pbio.0020398.

892 89. Chakrabortee, S., Byers, J.S., Jones, S., Garcia, D.M., Bhullar, B., Chang, A., She, R., Lee, L.,
893 Fremin, B., Lindquist, S., et al. (2016). Intrinsically Disordered Proteins Drive Emergence and
894 Inheritance of Biological Traits. Cell *167*, 369-381.e12. https://doi.org/10.1016/j.cell.2016.09.017.

895 90. Mitchell, A., Romano, G.H., Groisman, B., Yona, A., Dekel, E., Kupiec, M., Dahan, O., and Pilpel,
896 Y. (2009). Adaptive prediction of environmental changes by microorganisms. Nature *460*, 220–224.
897 https://doi.org/10.1038/nature08112.

898 91. Kussell, E., and Leibler, S. (2005). Phenotypic Diversity, Population Growth, and Information in
899 Fluctuating Environments. Science *309*, 2075–2078. https://doi.org/10.1126/science.1114383.

900 92. Masel, J. (2006). Cryptic Genetic Variation Is Enriched for Potential Adaptations. Genetics *172*,
901 1985–1991. https://doi.org/10.1534/genetics.105.051649.

902 93. Harvey, Z.H., Chakravarty, A.K., Futia, R.A., and Jarosz, D.F. (2020). A Prion Epigenetic Switch
903 Establishes an Active Chromatin State. Cell *180*, 928-940.e14.
904 https://doi.org/10.1016/j.cell.2020.02.014.

905 94. Lachowiec, J., Lemus, T., Thomas, J.H., Murphy, P.J.M., Nemhauser, J.L., and Queitsch, C. (2013).
906 The Protein Chaperone HSP90 Can Facilitate the Divergence of Gene Duplicates. Genetics *193*,
907 1269–1277. https://doi.org/10.1534/genetics.112.148098.

908 95. Alvarez-Ponce, D., Aguilar-Rodríguez, J., and Fares, M.A. (2019). Molecular Chaperones Accelerate
909 the Evolution of Their Protein Clients in Yeast. Genome Biol. Evol. *11*, 2360–2375.
910 https://doi.org/10.1093/gbe/evz147.

911 96. Wagih, O., and Parts, L. (2014). gitter: a robust and accurate method for quantification of colony
912 sizes from plate images. G3 Bethesda Md *4*, 547–552. https://doi.org/10.1534/g3.113.009431.

913 97. Meurer, M., Duan, Y., Sass, E., Kats, I., Herbst, K., Buchmuller, B.C., Dederer, V., Huber, F.,
914 Kirrmaier, D., Štefl, M., et al. (2018). Genome-wide C-SWAT library for high-throughput yeast
915 genome tagging. Nat. Methods *15*, 598–600. https://doi.org/10.1038/s41592-018-0045-8.

916 98. Bray, N.L., Pimentel, H., Melsted, P., and Pachter, L. (2016). Near-optimal probabilistic RNA-seq
917 quantification. Nat. Biotechnol. *34*, 525–527. https://doi.org/10.1038/nbt.3519.

918 99. Danecek, P., Bonfield, J.K., Liddle, J., Marshall, J., Ohan, V., Pollard, M.O., Whitwham, A., Keane,
919 T., McCarthy, S.A., Davies, R.M., et al. (2021). Twelve years of SAMtools and BCFtools.
920 GigaScience *10*, giab008. https://doi.org/10.1093/gigascience/giab008.

921 100. Nagalakshmi, U., Wang, Z., Waern, K., Shou, C., Raha, D., Gerstein, M., and Snyder, M. (2008).
922 The Transcriptional Landscape of the Yeast Genome Defined by RNA Sequencing. Science *320*,
923 1344–1349. https://doi.org/10.1126/science.1158441.

924 101. Zhao, R., Davey, M., Hsu, Y.-C., Kaplanek, P., Tong, A., Parsons, A.B., Krogan, N., Cagney, G.,
925 Mai, D., Greenblatt, J., et al. (2005). Navigating the Chaperone Network: An Integrative Map of
926 Physical and Genetic Interactions Mediated by the Hsp90 Chaperone. Cell *120*, 715–727.
927 https://doi.org/10.1016/j.cell.2004.12.024.

928 102. Luo, M., Meng, Z., Moroishi, T., Lin, K.C., Shen, G., Mo, F., Shao, B., Wei, X., Zhang, P., Wei, Y.,
929 et al. (2020). Heat stress activates YAP/TAZ to induce the heat shock transcriptome. Nat. Cell Biol.
930 *22*, 1447–1459. https://doi.org/10.1038/s41556-020-00602-9.

931 103. Diezmann, S., Michaut, M., Shapiro, R.S., Bader, G.D., and Cowen, L.E. (2012). Mapping the
932 Hsp90 genetic interaction network in Candida albicans reveals environmental contingency and
933 rewired circuitry. PLoS Genet. *8*, e1002562. https://doi.org/10.1371/journal.pgen.1002562.

934 104. Zhao, W., Zhang, S., Zhu, Y., Xi, X., Bao, P., Ma, Z., Kapral, T.H., Chen, S., Zagrovic, B., Yang,
935 Y.T., et al. (2022). POSTAR3: an updated platform for exploring post-transcriptional regulation
936 coordinated by RNA-binding proteins. Nucleic Acids Res. *50*, D287–D294.
937 https://doi.org/10.1093/nar/gkab702.

938 105. The UniProt Consortium (2023). UniProt: the Universal Protein Knowledgebase in 2023. Nucleic
939 Acids Res. *51*, D523–D531. https://doi.org/10.1093/nar/gkac1052.

940

941

Acknowledgments: We thank Joseph Schacherer for the 1,002 Yeast Genomes Project strain collection, Justin Smith for the CRISPR interference plasmid, and the Jarosz Lab for critical feedback and advice. This work was supported by the NIH (DP2-GM119140, RF1-AG057334, R01-AG06341801, and R01-HG012366 to D.F.J.; F32-GM125162 to C.M.J.), the National Science Foundation (NSF-MCB116762 to D.F.J.), the Swiss National Science Foundation (P2ZHP3_174735 to J.A.-R.), the European Molecular Biology Organization (ALTF 724-2018 to J.A.-R.), a Searle Scholar Award (14-SSP-210 to D.F.J.), a Kimmel Scholar Award (SKF-15-154 to D.F.J.), a Vallee Scholar Award (to D.F.J.) and a Discovery Innovation Award from Stanford University (to D.F.J.). D.F.J. is also a Science and Engineering Fellow of the David and Lucile Packard Foundation. Some of the computing for this project was performed on the Sherlock cluster. We would like to thank Stanford University and the Stanford Research Computing Center for providing computational resources and support that contributed to these research results.

Author contributions: C.M.J., J.A.-R., and D.F.J. conceived the project. C.M.J. performed pilot, mapping, genome editing, phenotyping, and transcriptomic experiments, designed and implemented the genetic mapping pipeline, performed transcriptomic and bioinformatic analyses, and prepared the figures. J.A.-R. performed pilot experiments, designed genome editing reagents, and performed genome editing experiments. C.M.J. wrote the original draft of the manuscript. C.M.J. and D.F.J. reviewed and edited the manuscript with input from J.A.-R.

Declaration of interests: The authors declare no competing interests.

963 **List of Supplemental Figures and Tables:**

964 Supplemental Figure S1: Related to Figure 1.

965 Supplemental Figure S2: Related to Figure 2.

966 Supplemental Figure S3: Related to Figure 3.

967 Supplemental Figure S4: Related to Figure 4.

968 Supplemental Figure S5: Related to Figure 5 and Figure 6.

969 Supplemental Figure S6: Related to Figure 7.

970 Supplemental Figure S7: Related to Method Details.

971 Supplemental Table S1: Stress conditions used in this study.

STAR METHODS

Resource availability

Lead contact

Further information and requests for resources and reagents should be directed to and will be fulfilled by Prof. Daniel F. Jarosz (jarosz@stanford.edu).

Materials availability

The original F_6 haploid genetic mapping panel is available from the National Collection of Yeast Cultures and the F_6 diploid mapping panel and all other yeast strains described here are available upon request to Prof. Daniel F. Jarosz (jarosz@stanford.edu).Bacterial strains bearing plasmids used here are likewise available upon request. Various CRISPEY gene editing plasmids are available from AddGene.

Data and code availability

All data supporting the findings of this study are available within the paper and its Supplemental Materials. All data required to recapitulate the mapping results and analyses are available at https://www.dropbox.com/scl/fo/0bx04fxbmzdm2tx63o2im/ACqBYF9kjZCe0DyLybhnJzU?rlkey=49cj84huufa5b2j7ikvamgigf&dl=0. All code required to generate the figures is available at https://github.com/cjakobson/hsp90-mapping. Upon publication a snapshot of the code and dependencies will be deposited as a Zenodo repository. RNA sequencing data are available at the Gene Expression Omnibus (GSE242925). Raw images of phenotyping experiments and custom code for cropping images and estimating spot sizes are available upon reasonable request to Prof. Daniel F. Jarosz (jarosz@stanford.edu).

993 **Experimental model details**

994 ***Yeast strains***

995 The construction and genotypes of the parents of the F_6 haploid collection, RM11 and YJM975,
996 are described in She and Jarosz[31]. Briefly, the F_6 diploids used here were constructed by mating
997 *leu⁻HYG*^{R} and *LEU*$^+$*hyg*^{S} F_6 haploid isolates genotyped previously[31] on YPD agar [RPI] followed
998 by selection for diploidy on synthetic defined medium lacking leucine [Sunrise] and supplemented
999 with 200 mg/L hygromycin. These F_6 diploids were arrayed into 384-well microtiter plates for
1000 cryostorage in SD-Leu+Hyg with 15% glycerol. All robotic manipulations were carried out using
1001 a Singer ROTOR pinning robot. The RM11 and YJM975 haploid parents of the original genetic
1002 cross bear auxotrophies used to facilitate crossing that are not present in the final F_6 diploid
1003 mapping panel. To avoid undesired interactions with these auxotrophies during validation
1004 experiments, reconstructions of Hsp90-interacting alleles were carried out in strains YDJ6635
1005 (YJM975a from the SGRP haploid collection[32]) and YDJ6649 (a spore derived from diploid
1006 RM11a/α), both of which are auxotrophic only for uracil. Key yeast strains and plasmids are listed
1007 in the **Key Resources Table**.

1008 ***Yeast culture conditions***

1009 Unless otherwise noted, yeast were propagated and phenotyped in minimal glucose medium
1010 consisting of 6.7 g/L yeast nitrogen base [RPI] and 20 g/L glucose [Sigma] supplemented with 20
1011 mg/L uracil [Sigma] to satisfy the lone auxotrophy of the F_6 diploid panel. Prior to phenotyping
1012 experiments, diploid strains were revived from frozen stocks in liquid SD-Leu+Hyg medium in
1013 384-well microtiter plates, propagated 24 hr at 30°C, then pinned to 1536-spot arrays on minimal
1014 glucose agar PlusPlates [Singer] and grown for 24 hr – 48 hr at 30°C. 1536-spot source plates
1015 prepared as described above were replicated to conditions as indicated using a Singer ROTOR

1016 pinning robot. Plates were incubated at 30°C and imaged at 24 hr intervals using an Epson V800
1017 scanner. Images were cropped using custom R scripts and spot sizes were quantified using the
1018 *gitter* R package. Colony sizes were extracted for genetic mapping using custom MATLAB scripts.
1019 Working concentrations for the various environmental perturbations are described in
1020 **Supplemental Table S1**.
1021
1022 **Method details**
1023 **v-Src *assay for Hsp90 activity***
1024 *v-Src* was expressed under the control of a galactose-inducible promoter from PDJ308 in the F_0
1025 heterozygous diploid YDJ5924. Cells were grown on solid medium containing either 2% glucose
1026 (repressing) or 2% galactose (inducing) as the sole carbon source and with or without 10 μM
1027 radicicol; Images were cropped using custom R scripts and spot sizes were quantified using the
1028 *gitter* R package[96].
1029 ***Western blotting***
1030 Cell lysis was conducted by bead beating in 20% trichloroacetic acid for 10 min at 50 Hz. Cell
1031 mass was normalized by optical density prior to lysis; approximately 1 OD-mL of cell mass was
1032 used per sample. Protein was precipitated for 30 min at ~23,000 x g at 4°C and the precipitate was
1033 resuspended in Tris pH 7.5 with 2% SDS before denaturation at 95°C for 5 min. Polyacrylamide
1034 gel electrophoresis was performed using 12-20% gradient gels at 120 V for 75 min. Proteins were
1035 transferred to PVDF membranes in Towbin transfer buffer for 2 hr at 100 V. Membranes were
1036 blocked with rehydrated milk, probed overnight at 4°C, and developed using WestFemto
1037 chemiluminescent substrate. Matched gels loaded with equal sample volumes were stained with
1038 Coomassie brilliant blue in parallel to western blotting. When required for reprobing, membranes

1039 were stripped of primary and secondary antibodies by boiling in Tris-buffered saline for 5 min.
1040 Antibodies are listed below.

1041 ***Genome editing using CRISPEY***

1042 Oligonucleotides containing appropriate guide and donor sequences for CRISPEY editing were
1043 designed as described by Sharon and colleagues[35] using code provided in that study. Oligos were
1044 designed separately for RM11 to YJM975 and YJM975 to RM11 mutations to account for
1045 differences in guide and template sequences due to neighboring polymorphisms (see **Key**
1046 **Resources Table**). SRR800790 and SRR1569760 were used as reference genomes for YJM975
1047 and RM11, respectively. Gene editing was conducted largely as described in Sharon and
1048 colleagues[35]. Briefly, dsDNA was synthesized from oligos by PCR, dsDNA fragments were
1049 inserted into the NotI-digested PDJ2318 editing plasmid by isothermal assembly using a 2xHiFi
1050 Assembly kit, and the ligated DNA was transformed into chemically competent *E. coli*. Gene
1051 editing of yeast was performed by transformation of the editing plasmid and selection on SD-Ura
1052 followed by 24h of growth in synthetic galactose medium lacking uracil. From these editing
1053 reactions, yeast cells were streaked to single colonies on YPD plates followed by restreaking to 5-
1054 FOA plates to cure the editing plasmid. Single colonies were genotyped by PCR and Sanger
1055 sequencing of the desired edited locus; screening two colonies per edit was typically sufficient to
1056 recover an edited clone.

1057 ***Homozygous diploid mRNA sequencing***

1058 Cell were grown in triplicate in minimal media as described above with and without 10 μM
1059 radicicol and harvested at OD ~ 0.8-1.0. Cell pellets were snap-frozen and stored at -80°C before
1060 submission to BGI for RNA extraction, polyA enrichment, reverse transcription, and sequencing,
1061 as described above for allele-specific expression analysis. Transcript abundance was again

1062 estimated using *kallisto*. Transcripts per million (TPM) estimates agreed well between replicates
1063 [**Fig. S7**]. Results are summarized in **Supplemental Table S4**.

1064 ***CRISPR interference***

1065 CRISPRi plasmids were cloned as described in Smith *et al.* Briefly, the anti-*ERG11* guide RNA
1066 sequence was ordered as an ssDNA oligonucleotide and amplified using extension primers as
1067 described in[83]. The CRISPRi plasmid (p416gT-Gal4-dCas9-Mxi1) was opened with NotI and the
1068 anti-*ERG11* guide inserted by isothermal assembly using a 2xHiFi Assembly kit, and the ligated
1069 DNA was transformed into chemically competent *E. coli* to create PDJ2494. After transformation
1070 into *S. cerevisiae* alongside a matched control plasmid with a non-targeting gRNA (PDJ397),
1071 strains were pre-grown for 24 hrs in the appropriate concentration of anhydrotetracycline (aTc) to
1072 establish steady-state knock-down then subjected to phenotyping under the appropriate aTc
1073 concentrations as described. Knock-down of Erg11 was quantified using a C-terminal fusion of
1074 mNeonGreen to the *ERG11* ORF[97].

1075

1076 **Quantification and statistical analysis**

1077 ***Genetic mapping***

1078 Prior to analysis, colony sizes were normalized to mean 0 and variance 1 (*i.e.* Z-scored) and filtered
1079 for outliers attributable to missing spots or debris (due to occasional pinning errors or image
1080 artifacts). Trait vectors were filtered for strains with an excess of missing genotypes and markers
1081 with insufficient genotype coverage were excluded. Statistical genetic mapping was performed
1082 essentially as described previously[30], with the difference that in the present work we mapped the
1083 change in the Z-scored trait for each segregant in each condition with and without 10 μM radicicol
1084 treatment. Briefly, coarse mapping was conducted by sequential stepwise selection on the

1085 homozygous followed by full (homozygous and heterozygous) genotype matrices. Fine mapping
1086 was conducted by ANOVA on *in silico* allele swaps as described in She and Jarosz 2018[31]. The
1087 genotype matrix included geometric pseudogenotypes corresponding to edge wells and to capture
1088 systematic plate-to-plate variability. Loci that were fine-mapped for one trait were inferred to be
1089 the underlying causal variant for other traits in which they were the lead candidate.

1090 ***1002 Genomes yeast strains and phylogenetic analysis***

1091 Genotype information for the 1,002 Genomes collection and the corresponding yeast strains[33] were
1092 a generous gift of Joseph Schacherer (Univ. of Strasbourg). Frozen stocks were revived and
1093 phenotyping experiments performed as described above for the F_6 diploid mapping panel. Growth
1094 measurements and quantification were conducted by optical scanning of Singer PlusPlates using
1095 *gitter* and custom code as described above.

1096 ***Allele-specific expression analysis***

1097 Cells were grown in triplicate in minimal media as described above with and without 10 μM
1098 radicicol and harvested at OD ~ 0.8-1.0. Cell pellets were snap-frozen and stored at -80°C before
1099 submission to BGI (www.bgi.com/us/home) for RNA extraction, polyA enrichment, reverse
1100 transcription, and sequencing. Transcript abundance was estimated using *kallisto*[98] and read counts
1101 per-site were estimated with *bcftools*[99] from *kallisto* pseudo-alignments. Allele-specific expression
1102 was called per-site based on a binomial test against the prior of major allele frequency = 0.5, with
1103 genome-wide Bonferroni correction based on the number of transcribed biallelic sites. Indels were
1104 excluded. After per-site calling, SNPs were assigned to genes and genes were assigned allelic
1105 imbalances if any SNP associated with their transcript exhibited significant allele-specific
1106 expression in any of the three replicate sequencing samples. Allelic imbalances agreed well
1107 between replicates [**Fig. S7**]. Results are summarized in **Supplemental Table S3**. Sensitivity

1108 estimates were conducted based on a sliding simulated read depth followed by binomial tests, with
1109 mock Bonferroni correction performed assuming the true number of transcribed biallelic sites in
1110 the hybrid diploid.

1111 ***Bioinformatic resources and enrichment analyses***

1112 Genomic analyses used the *S. cerevisiae* R64 reference genome unless otherwise noted.
1113 Transcription start and end sites were retrieved from[100]. Targets of sequence-specific transcription
1114 factors were retrieved from[39]. Predicted kinase targets were retrieved from[38]. Enriched TF hits
1115 were logically connected to Hsp90 function: Mig1[101] and Pdr1[25] interact with Hsp90; Hsp90
1116 inhibition downregulates Met4 targets[7]; and Yap1[102] and Stb5[103] homologues interact with Hsp90
1117 in other species. Modified alleles at targets of Pdr1 and Stb5 were enriched for fitness effects in
1118 fluconazole, consistent with the role of these TFs in multidrug resistance. Although several E3
1119 ligases exhibited modest enrichments for BioGRID physical interactors, only three (Etp1, Siz1,
1120 and Ssm4) were significant ($q < 0.05$) after multiple-testing correction. We also examined the
1121 targets of RNA-binding proteins based on PAR-CLIP and other interaction data (from the
1122 POSTAR3 database), but did not observe any significant enrichments ($q < 0.05$) after multiple-
1123 testing correction[104]. Gene and protein descriptions and GO terms were retrieved from SGD[71] and
1124 UniProt[105]. Predicted protein structures were retrieved from the AlphaFold Protein Structure
1125 Database[51]. Gene age estimates were retrieved from[78]. Haploinsufficient genes in *S. cerevisiae*
1126 were retrieved from[84]. pLoF data was retrieved from[85]. Haploinsufficient genes in human
1127 embryonic stem cells were retrieved from[86].

1128 **Key Resources Table**

REAGENT or RESOURCE	SOURCE	IDENTIFIER
Antibodies		
Anti-Hsp104	Enzo Life Sci.	ADI-SPA-1040
Anti-Pgk1	Invitrogen	22C5D8
Chemicals		
Yeast nitrogen base	RPI	Y20040
Glucose	Fisher	D16-3
Uracil	Sigma	U0750
Agar	IBI	IB49170
Maltose	Sigma	M9171
Raffinose	RPI	R20500
Ethanol (95%)	Fisher	04-355-226
4-nitroquinoline 1-oxide [4-NQO]	Sigma	N8141
Doxorubicin	Cayman	15007
Fluconazole	TCI	F0677
Lithium chloride	Acros	AC19988
Nickel sulfate	Sigma	227676
Rapamycin	Cayman	13346
Tebuconazole	Santa Cruz	SC204906
Deposited data		
mRNA sequencing data	This study	Gene Expression Omnibus (GSE242925)
Genetic mapping data	This study	Zenodo repository available upon publication.
Organisms/strains		
F_6 diploid progeny derived from RM11 x YJM975	Jakobson and Jarosz[30]	n/a
YJM975 haploid *LEU*$^+$*HIS*$^+$*ura*$^-$ *MATa*	Liti *et al.*[32]	YDJ6635
RM11 haploid *LEU*$^+$*HIS*$^+$*ura*$^-$ *MATα*	This study	YDJ6649
RM11/YJM975 F_0 heterozygous diploid	This study	YDJ5924
YJM975 haploid *LEU*$^+$*HIS*$^+$*ura*$^-$ *MATa AVO3*^{Lys1342Thr}	This study	YDJ8426
RM11 haploid *LEU*$^+$*HIS*$^+$*ura*$^-$ *MATα AVO3*^{Thr1342Lys}	This study	YDJ8428
YJM975 haploid *LEU*$^+$*HIS*$^+$*ura*$^-$ *MATa ERG11*^{T122014C}	This study	YDJ8281
RM11 haploid *LEU*$^+$*HIS*$^+$*ura*$^-$ *MATα ERG11*^{C122014T}	This study	YDJ8280
YJM975 haploid *LEU*$^+$*HIS*$^+$*ura*$^-$ *MATa NFS1*^{T92671C}	This study	YDJ9255
YJM975 haploid *LEU*$^+$*HIS*$^+$*ura*$^-$ *MATa ERG11*^{Asn433Lys}	This study	YDJ8436
YJM975 haploid *LEU*$^+$*HIS*$^+$*ura*$^-$ *MATa ERG11*$^{T122014C/Asn433Lys}$	This study	YDJ8437
Oligonucleotides		

AVO3 RM>YJM GAGTTACTGTCTGTTTTCCTTGAAAGGATATGA TTGCCTAGCTGACTTACTATATGTAGTACCTTG CTCTCGATGGAGTCATCGTCATTGCGGTATTGT GTAACATAGGGAGAAGAAAGGAGGAAACCCG TTTCTTCTGACGTAAGGGTGCGCAATGTAGTAC CGTGCTCTCGAGTTTCAGAGCTATGCTGGAA	This study	CMJP595-597+CMJP602-603
AVO3 YJM>RM GAGTTACTGTCTGTTTTCCTTGAAAGGATATGA TTGCCTAGCTGACTTACTATATGTAGTACCGTG CTCTCGATGGAGTCATCGTCATTGCGGTATTGT GTAACATAGGGAGAAGAAAGGAGGAAACCCG TTTCTTCTGACGTAAGGGTGCGCAATGTAGTAC CTTGCTCTCGAGTTTCAGAGCTATGCTGGAA	This study	CMJP595-597+CMJP604-605
ERG11^{122014} RM>YJM GAGTTACTGTCTGTTTTCCTATGGAGGGCAATT TTTAGAGGCTTTTCGAATACATGCGAGTACGTA AACGTCGTTAACTCGTGGAGATGCACAATAGG ATGTGCTCATATCAAGAAAAAAAGGAAACCCG TTTCTTCTGACGTAAGGGTGCGCAACGTAAAC GCCGTTAACTCGGTTTCAGAGCTATGCTGGAA	This study	RM_SNP_4
ERG11^{122014} YJM>RM GAGTTACTGTCTGTTTTCCTATGGAGGGCAATT TTTAGAGGCTTTTCGAATACATGCGAGTACGTA AACGCCGTTAACTCGTGGAGATGCACAATAGG ATGTGCTCATATCAAGAAAAAAAGGAAACCCG TTTCTTCTGACGTAAGGGTGCGCAACGTAAAC GTCGTTAACTCGGTTTCAGAGCTATGCTGGAA	This study	YJM_SNP_4
ERG11^{433} YJM>RM GAGTTACTGTCTGTTTTCCTCGTAATCGACTTC TTCACCGACGGAATAAGAGGAGGCAGAATCTT TGTTCCAACGGTGAATGTTGAATTGGTGAGCA TTAGGGAAGTATTCGTCTCTTAAAGGAAACCC GTTTCTTCTGACGTAAGGGTGCGCAAGGCAGA ATCGTTGTTCCAAGTTTCAGAGCTATGCTGGA A	This study	CMJP670
NFS1 YJM>RM GAGTTACTGTCTGTTTTCCTAATTGCACTTTAA CATTAATATTGACAAGGAGGAGGGCACCACAC AAAAAGTTAGGTGTAACAGAAAATCATGAAAC TATGATTTCTAATTTATATATTGAGGAAACCCGT TTCTTCTGACGTAAGGGTGCGCAAGGGCATCA CACAAAAAGTTGTTTCAGAGCTATGCTGGAA	This study	CMJP718
anti-*ERG11* gRNA ctgggagctgcgattggcagATAATTTACCAATAACGAAA gttttagagctagaaatagc	Smith *et al.*[83]	CMJP769

CRISPRi extension primer 1 gactagccttattttaacttgctatttctagctctaaaac	Smith *et al.*[83]	CMJP770
CRISPRi extension primer 2 tcgcggctgggaacgaaactctgggagctgcgattggcag	Smith *et al.*[83]	CMJP771
Recombinant DNA		
pRS316 CEN Cb/URA3 pGAL::v-Src	D. Morgan (UCSF)	PDJ308
CRISPEY editing vector *pEASY CEN Cb/URA3 pGAL::Cas9 pGAL::RT Ec86 pGAL::sgRNA::template*	This study	PDJ2318
CRISPRi control vector *pRS416 CEN Cb/URA3 pTEF1::dCas9::Mxi1 pRPR1:gRNA (non-targeting)*	Smith *et al.*[83]	PDJ397
anti-*ERG11* CRISPRi *pRS416 CEN Cb/URA3 pTEF1::dCas9::Mxi1 pRPR1:gRNA (anti-ERG11)*	This study	PDJ2494
Software and algorithms		
Custom genetic mapping code	This study	https://github.com/cjakobson/hsp90-mapping
Gitter	Wagih and Parts[96]	https://omarwagih.github.io/gitter/
Kallisto	Bray *et al.*[98]	https://pachterlab.github.io/kallisto/
Bcftools	Danecek *et al.*[99]	https://samtools.github.io/bcftools/bcftools.html

1129

1130 **List of Other Supplemental Items:**

1131 Supplemental Table S2: Summary of genetic mapping results.

1132 Supplemental Table S3: Allele-specific expression data.

1133 Supplemental Table S4: Homozygous diploid mRNA expression data.